10-1-1984

An airborne thermal remote sensing calibration technique

I. D. Macleod

An Airborne Thermal Remote Sensing Calibration Technique

by

I.D. Macleod
Mech. Eng. Royal Military College 1977
P.Eng Association of Professional Engineers Ontario 1978

A thesis submitted in partial fulfillment
of the requirements for the degree of
Masters of Science in the School of
Photographic Arts and Sciences in the
College of Graphic Arts and Photography
of the Rochester Institute of Technology

October, 1984

Signature of the Author _____
Photographic Science and Instrumentation

Accepted by _____
Coordinator, Graduate Program

College of Graphic Arts and Photography
Rochester Institute of Technology
Rochester, New York

CERTIFICATE OF APPROVAL

M.S. DEGREE THESIS

The M.S. Degree Thesis of Ian D. Macleod
has been examined and approved
by the thesis committee as satisfactory
for the thesis requirement for the
Master of Science degree

Dr. J.R. Schott, thesis advisor

Dr. E.M. Granger

Dr. W. Brouwer

DATE 10/31/94

THESIS RELEASE PERMISSION FORM

ROCHESTER INSTITUTE OF TECHNOLOGY
COLLEGE OF GRAPHICS ARTS AND PHOTOGRAPHY

Title of Thesis: AN AIRBORNE THERMAL REMOTE SENSING CALIBRATION TECHNIQUE

I, Captain Ian Douglas Macleod, prefer to be contacted each time a request for reproduction is made. I can be reached at the following address:

NDHQ/DASP 5
101 Colonel By Drive
Ottawa, Ontario
Canada
K1A 0K4

date: 01 OCTOBER 1984

An Airborne Thermal
Remote Sensing
Calibration Technique

by

Ian D. Macleod

Submitted to the
Photographic Science and Instrumentation Division
In partial fulfillment of the requirements
for the Master of Science degree
at the Rochester Institute of Technology

Abstract

A calibration technique for airborne thermal remote sensing systems without the requirement for ground truth or multiple altitude measurements is developed and evaluated. This technique is based on vertical and offset look angles and in effect corrects for image degradation due to atmospheric effects.

The results were evaluated by comparison to a multiple altitude regression technique using previously generated imagery, and by statistical methods, including an error analysis. Assuming that the multiple altitude regression technique was exact, the error on apparent temperature produced by this angular technique was 0.32°C.

ACKNOWLEDGEMENTS

Most sincere thanks are extended to the many people behind the scenes who offered support and inspiration throughout the project. Their help was greatly appreciated.

In particular I would to thank the following:

-- the research staff at the Rochester Institute of Technology Wallace Memorial Library for their assistance in the literature search.

--the personnel at Calspan Corporation for the loan of their material and equipment. The project would not have been possible without the thermal imagery they so graciously provided.

-- the Canadian Armed Forces for the administrative and financial support. In particular thanks to the offices of DIT, DATES and especially DACS who provided sponsorship for this course.

-- the members of my thesis committee for their expertise and guidance.

I would like to offer special thanks to the following personnel for their valued help in completing this project:

-- the Coordinator of Graduate Studies in the Photographic Science and Instrumentation Department, Dr. R.L. Francis, whose motivation and technical advice were invaluable.

-- Joe Biegle for his assistance in determining methods of working through the many problems encountered throughout the project.

-- Dr. J.R. Schott whose remote sensing background and innovative ideas were a true inspiration in undertaking the study.

-- and lastly, my wife Anne and son Andrew whose love, encouragement and patience were such an asset during the many periods of hardship.

TABLE OF CONTENTS

LIST OF TABLES

LIST OF FIGURES

LIST OF SYMBOLS

a - absorption coefficinet

A - proportionality constant

b - Y axis intercept

BB - blackbody

c - velocity of light

D - density

g - gain

h - height

H - Plancks' constant

k - Boltzmans' constant

m - slope

n - number of points

P - flux transmitted

P_0 - flux incident

R - object reflectance

R^2 - correlation coefficient

RSS - residual sum of squares

SSR - regression sum of squares

SXX - sum of squares - X

SYY - sum of squares - Y

SXY - sum of squares - XY

S^2 - variance

$S(X)$ - error of variable X

T - temperature

v - velocity

V - voltage

V_0 - initial voltage

W - spectral radiant emittance

W_A - path radiance

W_0 - apparent radiant emittance

W_S - sky radiant emittance

W_T - blackbody equivalent radiant emittance

X - path length

y - distance on the image from nadir line to point p

α - fraction absorbed incident energy

ε - emissivity

σ - Stefan-Boltzman constant

π - pi

λ - wavelength

τ - transmission

μ - micro-meter

ϕ - view angle

ϕ_p - instantaneous field of view

ρ - fraction reflected incident energy

SECTION 1

1.1 Introduction

Considerable interest in thermal remote sensing has been generated due to a wide variety of applications. This is because temperature is one of the principle controls on virtually all physical, chemical and biological processes in the environment.[11] Earth resource management activities are one primary area of interest and if any detailed or legal action is necessary, a quantitative study must be carried out. Therefore, a radiometrically calibrated system is a requirement.

Normally temperature measurement is thought of as involving some measurement instrument being placed in contact with, or immersed in, the body whose temperature is to be measured. This measure is in reality 'kinetic temperature' or the internal temperature of the body.[11,27] With thermal remote sensing, radiant temperature or the external energy radiated as a function of temperature is detected and measured. However, because this energy is detected from a distance, the medium through which the energy travels is involved. This medium is usually the atmosphere when airborne thermal remote sensing is utilized.

Atmospheric effects have been found to be very detrimental on image quality and many techniques have been developed to reduce these effects. Some are very complicated, involving high technology and considerable expense. Other simple models need to be developed for the small user, who cannot afford the cost and effort of the more elaborate models.

Atmospheric effects have been studied in both the visible and thermal regions of the electromagnetic spectrum. Thermal infrared energy cannot be detected by photographic film because of the long wavelengths involved (8-14 μm), and electronic detectors must be used. This results in parameters different from a photographic system and therefore a calibration technique must be developed specifically for thermal imaging systems.

In this study, a simple and inexpensive technique accounting for image degradation in the thermal infrared spectral region, due to atmospheric effects is developed and evaluated.

1.2 Background

Thermal remote sensing calibration techniques have not been investigated in great depth because of the nature of user interpretation. It has been common practice to compare thermal imagery in a relative fashion and not to use a totally quantitative approach.[11]

However, some serious attempts at thermal calibration have been undertaken. Atmospheric absorption was considered as early as 1942, when E. Elassen[8] presented a paper on the then present state of the art. This paper dealt mainly with models for CO_2 and H_2O absorption bands.

After World War II, many papers were written on the subject of infrared transmission through the atmosphere. A major laboratory study was begun at Ohio State University to investigate absorption bands which later included the use of controlled or synthetic atmospheres.[7]

In 1951, Yates calculated transmissions through various atmospheres of the radiation of blackbodies with different temperatures.[8] Many further studies have since been carried out on atmospheric attentuation and absorption bands.

One of the first to attempt an actual thermal airborne calibration was Saunders in 1967.[19] His method estimated the influence of air layers and reflectivity simultaneously. Saunders based his method on the premise that if the line of sight is inclined at an angle θ to the vertical, the effective mass of absorbing gas measured down from the flight altitude to the level z can be written as $u(z) \sec \theta$ where $u(z)$ is the effective mass measured down in the vertical direction. After

simplifying he formulated that a radiometric measurement of the water surface at an angle of 60° from the normal doubles the influence of the air layer and reflectivity. Saunders admits that doubling gives a slight underestimation theoretically and this places some doubt on the accuracy. Also the approach of obtaining imagery at 60° poses some geometric problems practically for the system. He concluded the difference between a normal and 60° measurement is the only correction required and his best estimates of the accuracy were ± 0.2°C.

In 1968, Lorenz[13] discussed a radiometric method for surface temperature measurements, with emphasis on possible errors of this method. He showed that for a certain flight level, the most important factors influencing radiometer measurements are surface and air temperatures, whereas variations in the humidity and the temperature gradient of the air layer between the target and radiometer are less important. Lorenz produced a set of correction curves based on the differences between surface temperature and air temperature at constant relative humidity and altitude. For this method, the temperature at flight level is required and he claimed accuracy of ± 1°C. For practical use, Lorenz assumed that the air temperature near the radiometer was indicative of the much lower radiation temperature of the clear sky. Thus he is only estimating skylight effects and accuracy here may be effected.

Weiss (1971)[27] carried out a study dealing with atmospheric windows. He claimed that error can be minimized by working in the window at 10-12 μm rather than utilizing the full window at 8-14 μm. Comparison of the data showed the measured error to be reduced 1.5-2.0 times with the narrow bandpass. The comparison was done using two radiometers flown side by side over water and land. He also showed that the curves

of altitude vs. radiometer reading were approximately linear below 1070 m altitude and from this, he hypothesized that a straight line extrapolation at two different altitudes would provide a means of obtaining surface temperatures. The validity of a two point extrapolation however is questioned here, in that two points do not provide a large data base. His resultant errors were 0.5°C for 10-12 μm region and 0.8°C for 8-14 μm up to an altitude of 300 m. He did however, have some difficulty with unexplained aerosol effects due to his location in Barbados. Also, he completely ignored sky reflection which places doubt on the whole method.

Prabhakara et al. (1974)[17] devised a technique based on the differential absorption properties of water vapour. They used a two channel radiometer to determine the water vapour absorption correction, without detailed knowledge of the vertical profiles of temperature and water vapour. Aerosol effects were not explicitly considered and Prabhakara developed this technique specifically to measure sea surface temperatures. Using data from a Nimbus infrared interferometer spectrometer (IRIS) they simulated measurements to select wavelengths with different total absorption. The best accuracy they obtained was 1.0°C. This model has been criticized[15] because it was discovered that different models required different bandwidths for the best results.

McMillan (1975)[15] carried Prabhakara's procedure further in adding a component proportional to the partial pressure of water vapour. He also modelled measurements at two angles rather than two wavelengths. McMillan concentrated on moist atmospheres and sea surface temperatures and he utilized forecast atmospheres, i.e., a set of 32 atmospheres, as

standards. In an operational system, the true atmosphere would not be known and the accuracy would be in doubt.

Chedin et al. (1981)[8] used the double viewing angle method for determination of sea surface temperature from two satellites. It proved to be a promising technique but the drawback of the method was the added complexity of the spacecraft sensor system.

The techniques reviewed up to this point have all been based simply upon a correction factor between two data points. They are designed for then applying this correction factor and extrapolating to zero altitude to get a reading of true surface temperature. They are not necessarily valid for anything but the conditions under which the measurements were made (i.e. if certain angles were used then temperature corrections are only valid for those angles). A different concept was undertaken in this study in that the correction was included in more universal equations (i.e. different angles could be used varying the data conditions). Also no extrapolations were required.

Schott (1977)[21] developed a different thermal remote sensing technique for measuring water surface temperatures from airborne platforms. The concept was based on a profile where thermal data was collected at various altitudes and this procedure provided an extrapolation to zero altitudes. Schott included both a radiometer profile technique and a scanner profile technique. The report incorporated corrections for flight parameters and also radiometer (scanner) calibrations. An angular calibration was utilized with the scanner to determine a correction needed due to radiant energy from the sky incident on the surface. The airborne results were checked by means of boats which measured actual temperatures and the measurements were within ± 0.70°F

of the actual temperature. This represents quite an acceptable error for most requirements considering this is a totally airborne approach. The drawback of this approach is that it requires flying at multiple altitudes over the same object in order to produce an accurate extrapolation to ground level. This can represent considerable expense in terms of flying time and labor.

Schott (1981)[24] carried this same approach further in evaluating Applications Explorer Mission A Data for NASA. Schott calibrated this Heat Capacity Mapping Mission to ± 0.4°C using the technique he developed in 1977.

Military interest in thermal remote sensing has also been responsible for some development in this field. FLIR (Forward looking infrared) sensors were developed for air-borne use first around 1960[12] and as time advanced, low noise, high resolution components have been added to the systems to improve image quality.

Recent trends have been towards more and more complicated models. For example, AFCRL LOWTRAN, developed by Air Force Cambridge Research Laboratories,[18] is an elaborate computer model for calculating infrared transmittance spectra. In particular, aerosols and water vapor scattering are being given a great deal of attention by these models. An experiment flown by Nimbus III and IV satellites dealt exclusively with atmospheric transmission and absorption bands.[18] These models require considerable amounts of money and resources which the smaller user cannot afford. Also, the complexity of these models leads to more time required for computation, and more variables being used.

Another aspect sometimes used to overcome the complicated models is to use ground truth. This involves setting up panels of known emissivity

that are large enough to be measured from the air. Scarpace[20] developed a classification system for thermal plumes using ground truth in the form of stirred water in swimming pools as well as one lake temperature. Scarpace states that caution must be exercised when assigning ground truth temperatures to the imagery because some isothermal regions corresponded to an area four times as large as the typical stated resolution for the scanner that was used. Further work was being attempted using Fourier Transform techniques to obtain a more precise image of the input. He achieved accuracies of 0.1°C with this technique.

The intent of this study was to devise a simple calibration technique particularly applicable to the small user, with an accuracy comparable to the more elaborate models. To date, the only similar technique is one developed by Saunders.[19] However Saunders' method involves an estimate at only one angle (60°) and therefore is only theoretically valid at 60°. He also used radiometric data with no imagery and based his measurement on water, for which specular reflection and rough surfaces could present a problem.

The technique developed for this study is different from Saunders in that:

1) actual thermal imagery is utilized
2) multiple angles are taken
3) many varying surfaces are measured
4) the theoretical equations are developed further in that more variables are accounted for.

The concept of this technique is simple. Measurements are made vertically and at various offset view angles of Lambertian objects along parallel flight lines. Only two images are required of several objects

and through calibration equations, atmospheric attenuation and path radiance can be determined. These can then be applied to the general case of all angles and true surface temperature can be determined without the use of ground truth. The results indicate that the technique has the potential to be successful and could be easily applied by the small user. It requires less flying time than previous methods and is relatively simple which makes this technique an attractive one.

SECTION 2

OBJECTIVES

The objectives of this study were as follows:

1. To develop a single altitude angular calibration technique, applicable to a totally airborne thermal remote sensing system in which atmospheric effects can be corrected.

2. Using previously generated imagery, apply this technique to calculate atmospheric transmittance, and path radiance and thereby produce a true reading of radiant temperature of the object.

3. To evaluate this technique by comparison with a multiple altitude regression technique and by statistical methods including an error analysis.

SECTION 3

THEORY

3.1 Theoretical Development of Equations

The physics of electromagnetic radiation can be described in accordance with the concepts of blackbody radiation. A blackbody is a hypothetical, ideal radiator that totally absorbs and re-emits all energy incident upon it.[9] Any object having a temperature greater than absolute zero emits radiation whose intensity and spectral composition are a function of the material type involved and the temperature of the object under consideration.[11] A family of blackbody curves is shown in Figure 1, illustrating how the energy peak shifts towards shorter wavelengths with increases in temperature. Of particular interest is the peak near 9 μm for 300°K,[21] where natural surfaces can be studied. The dominant wavelength or wavelength at which a blackbody radiation curve reaches a maximum is related to its temperature by Weins Displacement law.[11,28]

$$\lambda = \frac{A}{T} . \qquad (1)$$

where λ = wavelength of maximum spectral radiant emittance

$A = 2898\ \mu m\ ^{\circ}K$

T = temperature, °K

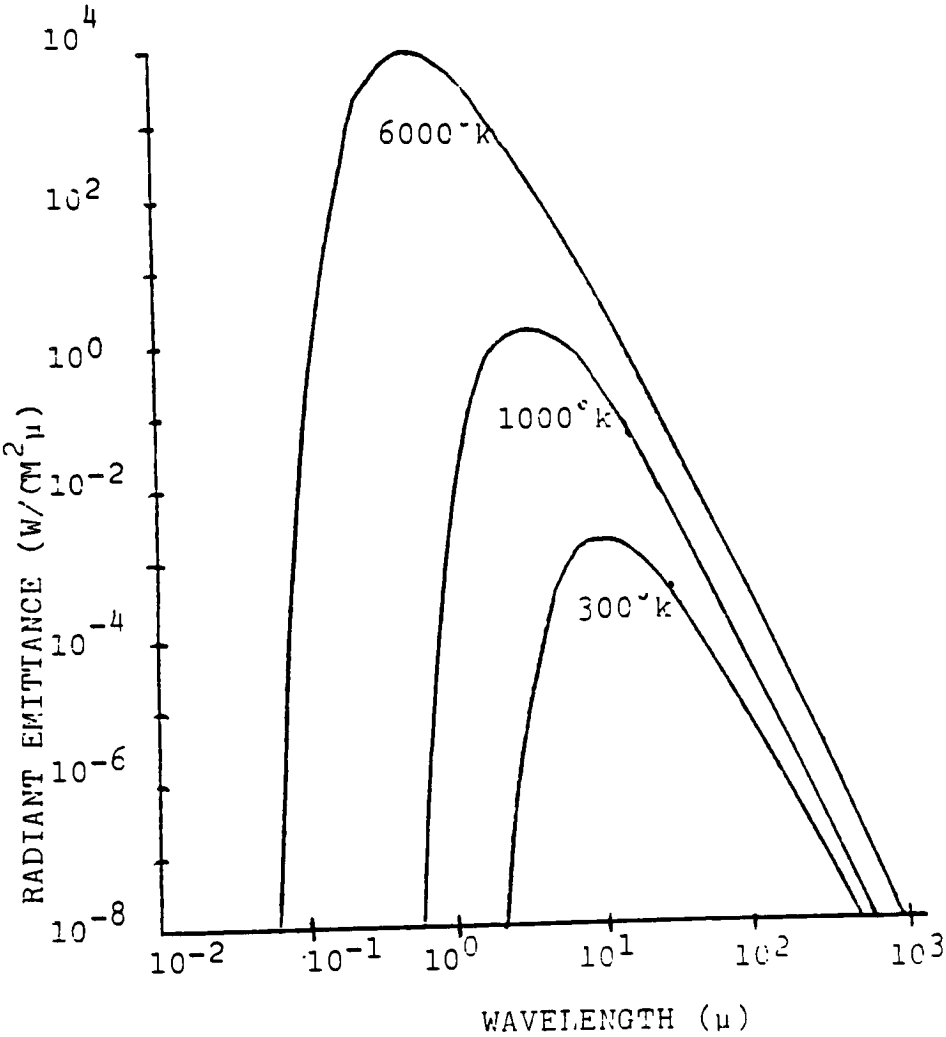

FIGURE 1

BLACKBODY CURVES

after SCHOTT (1976)

Plancks law describes the general form of the spectral distribution of the radiation from a blackbody as:

$$W_\lambda = 2c^2H\lambda^{-5}(\exp cH/\lambda kT-1)^{-1} \quad (2)$$

where W_λ = spectral radiance $Wcm^{-2}\ sr^{-1}$

λ = wavelength, μm

H = Planck's constant $(6.6256 \pm .0005) \times 10^{-34} Wsec^2$

T = absolute temperature °K

c = velocity of light $(2.997925 \pm .00003) \times 10^{10}$ cm sec^{-1}

k = Boltzman's constant $(1.38054 \pm .00018) \times 10^{-23}$ Wsec K^{-1}

Integrating Planck's law over wavelengths extending from zero to infinity gives an expression for the radiant emittance; the flux radiated into a hemisphere above a blackbody of unit area. This is commonly known as the Stefan-Boltzman law.

$$\pi \int_0^\alpha W_\lambda = W = \sigma T^4 \quad (3)$$

where W = radiant emittance W cm^{-2}

σ = Stefan-Boltzman constant $(5.6697 \pm .0029) \times 10^{-12}\ Wcm^{-2}{}^\circ K^{-4}$

Differentiating Planck's law and solving for the maximum gives Wein Displacement law (equation 1).

There is a problem however in using these equations for finding the dependence of W on temperature over a defined bandpass. To do this, Planck's equation (equation 2) must be integrated over the limits of the defined bandpass. This can be carried out using Simpson's rule to approximate the integral. Standard blackbody tables exist,[28] but Simp-

son's rule will be incorporated in this study for more accuracy at each specific temperature and to avoid interpolations.

All of the preceeding discussion dealt exclusively with perfect blackbodies as the model. In reality, most materials behave as gray bodies and are not perfect absorbers or radiators. To compensate, the factor of emissivity is introduced. Emissivity is a variable that describes how efficiently an object radiates energy compared to a blackbody at the same temperature.[10] A gray body has an emissivity of less than unity at all wavelengths.

$$W = \varepsilon W_T \tag{4}$$

where W = radiant emittance of the source

ε = emissivity

W_T = radiant emittance of a blackbody, at the same temperature as the source

When radiant energy is incident upon a surface, three processes can occur: a fraction, α, of the incident energy, may be absorbed, a fraction, ρ, may be reflected, and a fraction, τ, may be transmitted.[10] Since energy must be conserved, the following relationship will hold:

$$\alpha + \rho + \tau = 1 \tag{5}$$

By definition, a blackbody absorbs all the incident radiant energy so that $\alpha = 1$ and $\rho = \tau = 0$.[14] Kirchoff observed that at a given temperature, the ratio of radiant emittance of a graybody to absorptance is a constant for all materials and that it is equal to the radiant

emittance of a blackbody at that temperature.[9] Known as Kirchoff's law, it is stated as:

$$\frac{\varepsilon W}{\alpha} = \sigma T^4 \tag{6}$$

Using the Stefan-Boltzman law:

$$\frac{\varepsilon \sigma T^4}{\alpha} = \sigma T^4 \tag{7}$$

or

$$\varepsilon = \alpha \tag{8}$$

This is equivalent to saying that the emissivity of any material at any given temperature is numerically equal to its absorptance. Carrying this further, since an opaque material does not transmit energy, i.e. $\tau = 0$; therefore:

$$\varepsilon + \rho = 1 \tag{9}$$

When designing an infrared system, the effect of the earth's atmosphere must be considered as a major factor. The infrared radiation incident on an infrared receiver is nearly always extensively changed by the atmosphere intervening between it and the target. The intervening medium is an inhomogeneous and continuously changing mixture of gases, liquid droplets and particulate solid matter.[9] The gases of primary interest are water vapour (H_2O), carbon dioxide (CO_2), nitrous oxid (N_2O) and ozone (O_3).[9,10,28]

Within the earth's atmosphere, there is a transmission window between eight and fourteen μm as shown in Figure 2. This window encom-

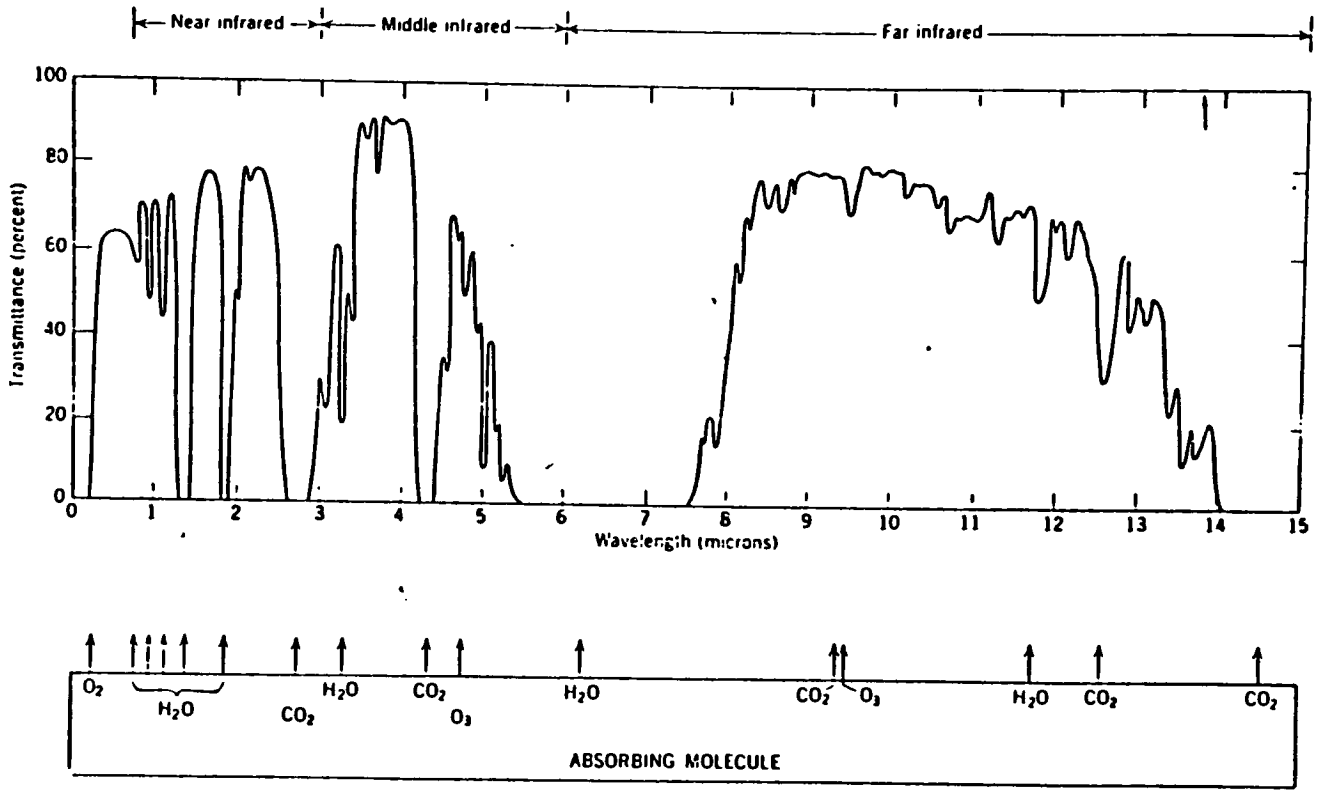

FIGURE 2

TRANSMISSION OF THE ATMOSPHERE OVER
THE ELECTROMAGNETIC SPECTRUM

after HUDSON (1969)

passes the radiant energy peak near 9 μm for objects near earth's ambient temperature of 300°K.

The primary attentuation in this window due to atmospheric effects leads to a transmission factor and a path radiance term which influence emissive radiation detected, i.e.:

$$W = \tau\varepsilon W_T + W_A \tag{10}$$

where W = observed radiance at the detector

τ = atmospheric transmission

W_A = path radiance

ε = emissivity

W_T = blackbody equivalent radiance from object itself

In addition, there is a certain amount of radiation which will be reflected from the ground that will reach the detector. This energy comes from the sky as shown in Figure 3. For this study, night imagery will be used and therefore effects from the sun will not be considered. Adding skylight reflection to Equation 10 provides the following:

$$W = \tau\varepsilon W_T + W_A + W_S\tau R \tag{11}$$

where W_S = radiance from sky incident on object

R = object reflectance

With this equation, it should be recognized that W_A and τ are dependent on the path length and therefore look angle between the detec-

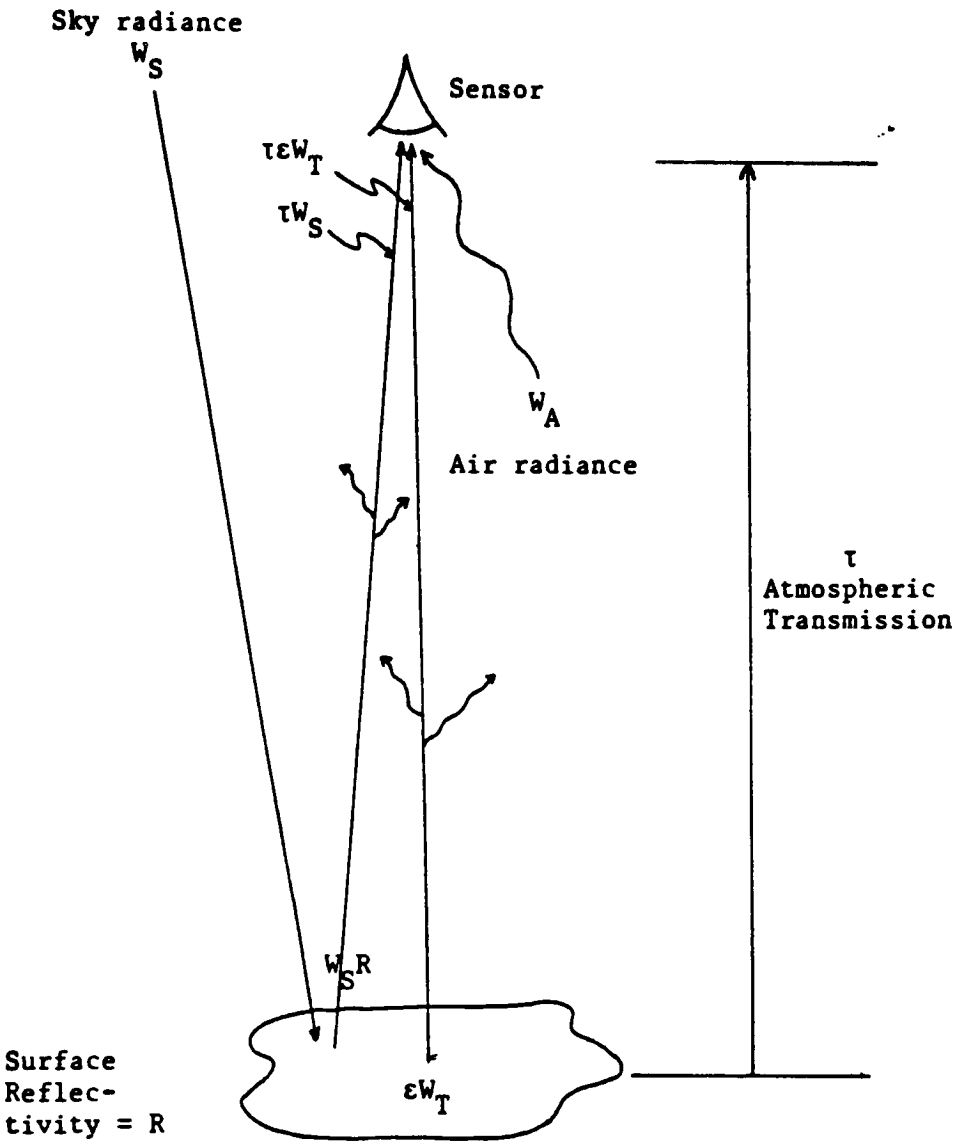

FIGURE 3
ENERGY PATHS

after SCHOTT (1981)

tor and the object (Figure 4). Similarly, reflection and emittance are dependent upon the look angle. Incorporating these into Equation 11 yields:

$$W(h,\Theta) = \tau(h,\Theta)\varepsilon(\Theta)W_T + W_A(h,\Theta) + \tau(h,\Theta)W_S R(\Theta) \quad (12)$$

or $$W(h,\Theta) = \tau(h,\Theta)W(0,\Theta) + W_A(h,\Theta) \quad (13)$$

where $$W(0,\Theta) = \varepsilon(\Theta)W_T + W_S R(\Theta) \quad (14)$$

Limiting the look angle to zero gives:

$$W(h,0) = \tau(h,0)\varepsilon W_T + \tau(h,0)W_S R + W_A(h,0) \quad (15)$$

or $$W(h,0) = \tau(h,0)W_0 + W_A(h,0) \quad (16)$$

where $$W_0 = \varepsilon W_T + W_S R \quad (17)$$

When comparing offset look angles to vertical angles, atmospheric transmission will vary as the angle changes. This relationship was originally investigated by Bouguer and rediscovered by Lambert and become know as the Bouguer-Lambert law.[10]

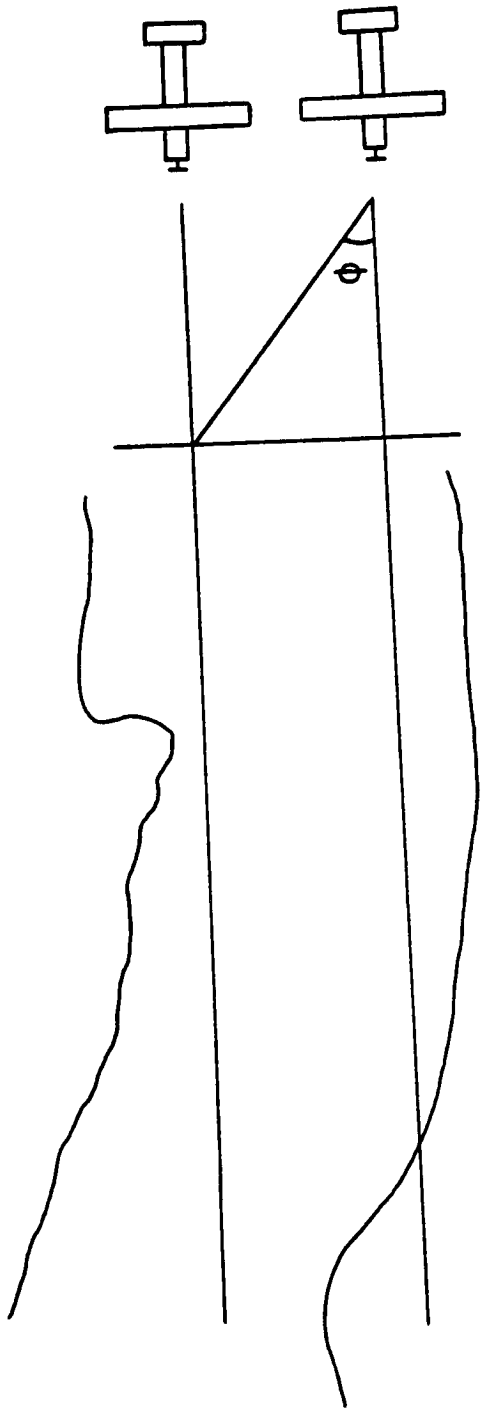

FIGURE 4
EXAMPLE OF PARALLEL FLIGHT LINES
SHOWING OFFSET LOOK ANGLES

$$\frac{P}{P_0} = e^{-ax} \tag{18}$$

where P/P_0 = transmittance of flux entering a layer

a = absorption coefficient

x = path length

If the look angle is changed, this is equivalent to changing path length and equation 18 could be re-stated as:

$$\tau(h,\Theta) = \tau(h,0)^{(\sec\Theta)} \tag{19}$$

Radiance will also change as look angle is varied, due to path length:

$$W_A(h,\Theta) \sim W_A(h,0)/\cos\Theta \tag{20}$$

This approximation was studied in depth after data was taken and it is detailed under Section 5.3.

A major assumption must be made at this point in that the material being measured is Lambertian in character; i.e. radiance is dependent of angle ($\varepsilon(\Theta) = \varepsilon(0)$ and $R(\Theta) = R(0)$). With the proper choice and careful selection of materials to be measured, this assumption is good and will not change the validity of this study. Preliminary experimentation was carried out to ensure that all objects utilized were Lambertian throughout a range of angles. Various materials were examined and all non-Lambertian materials were eliminated.

Using equations 19 and 20, and substituting in Equation 13:

$$W(h,\theta) = \tau(h,0)^{1/\cos\theta} W(0) + W_A(h,0)/\cos\theta \quad (21)$$

From equation 16:

$$W_0 = \frac{W(h,0)}{\tau(h,0)} - \frac{W_A(h,0)}{\tau(h,0)} \quad (22)$$

Substituting equation 22 in equation 21:

$$W(h,\theta) = \tau(h,0)^{1/\cos\theta} \left[\frac{W(h,0)}{\tau(h,0)} - \frac{W_A(h,0)}{\tau(h,0)}\right] + \frac{W_A(h,0)}{\cos\theta} \quad (23)$$

Expanding Equation 23:

$$W(h,\theta) = \tau(h,0)^{(1/\cos\theta-1)} W(h,0) - \tau(h,0)^{(1/\cos\theta-1)} W_A(h,0) + \frac{W_A(h,0)}{\cos\theta} \quad (24)$$

Simplifying:

$$W(h,\theta) = mW(h,0) + b \quad (25)$$

where $$m = \tau(h,0)^{(1/\cos\theta - 1)} \tag{26}$$

$$b = [(\frac{1}{\cos\theta}) - \tau(h,0)^{(1/\cos\theta - 1)}] W_A(h,0) \tag{27}$$

$$b = (\frac{1}{\cos\theta} - m)W_A(h,0) \tag{28}$$

In dealing with Equation 25, $W(h,\theta)$ and $W(h,0)$ can be measured. This was carried out by desitometrically reading thermal infrared imagery at the vertical angle and at a given offset angle and converting the densities through temperature to emittance. A series of $W(h,\theta)$ vs. $W(h,0)$ values enables a regression to be carried out on Equation 25, and with Equations 26, 27 and 28, $\tau(h,0)$ and $W_A(h,0)$ can be determined. Also, $\tau(h,\theta)$ and $W_A(h,\theta)$ for any look angle can be determined using Equations 19 and 20 respectively. This constituted the main thrust of this study.

This analysis can be carried further to determine actual surface radiance. Referring to Equation 12, W_S, $\varepsilon(\theta)$ and $R(\theta)$ would be required for this. If required, a technique developed by Schott[21] would enable W_S to be determined. However, this technique involves using tabulated values of $R(\theta)$ and $\varepsilon(\theta)$ for non-Lambertian surfaces. The non-Lambertian character is an advantage here in that a true variation of emissivity and reflection with angle will lead to a more accurate W_S value with Schott's[21] method.

Once W_T is determined by Equation 12, radiant temperature can be calculated by using Plancks equation integrated over 8-14 μm. This simply involves estimating a temperature, applying Planck's equation and comparing W calculated with the actual W_T. Then temperature is

incremented and W is again calculated. This process is continued until W calculated equals W_T, and this gives the final temperature. This technique was carried out to give temperature to an accuracy of 0.01°K.

Thus, it is theoretically possible to measure surface radiant emittance and thus surface temperature using only vertical and slant range measurements at a single altitude.

3.2 Sensing Systems

The two types of thermal systems used for this study were the thermal radiometer and thermal scanner. The first to be considered was the radiometer. This non-imaging device quantitatively measured and recorded the apparent radiant temperature of objects within its field of view.[8] The radiometer used for this study was a Barnes PRT-5, modified to provide a 2° field of view. A schematic is shown in Figure 5.[10] The output was fed to a multimeter and through a calibration graph of millivolts vs. temperature, the apparent temperature could be determined. Absolute calibration of the radiometer was not required for this study as relative readings only were taken. This instrument is characteristically high in sensitivity and is very accurate. The only main failings are low spatial resolution and the non-imaging output. For this study, the radiometer was used to measure one surface at a time, and the ability to distinguish objects was not important.

The main instrument for this study was a thermal line scanner. This device builds up a two dimensional record of radiant temperature data for a swath beneath an aircraft. The main components are shown in Figure 6.[10] This is an imaging device utilizing a scanning mirror. The detector must be cooled well below ambient temperature to minimize detector noise. It is highly sensitive and has a rapid response time.[11]

There is an inherent problem however with the scanning mirror, in that it produces scale distortions in the direction perpendicular to the flight path. As shown in Figure 7, if the mirror rotates with constant

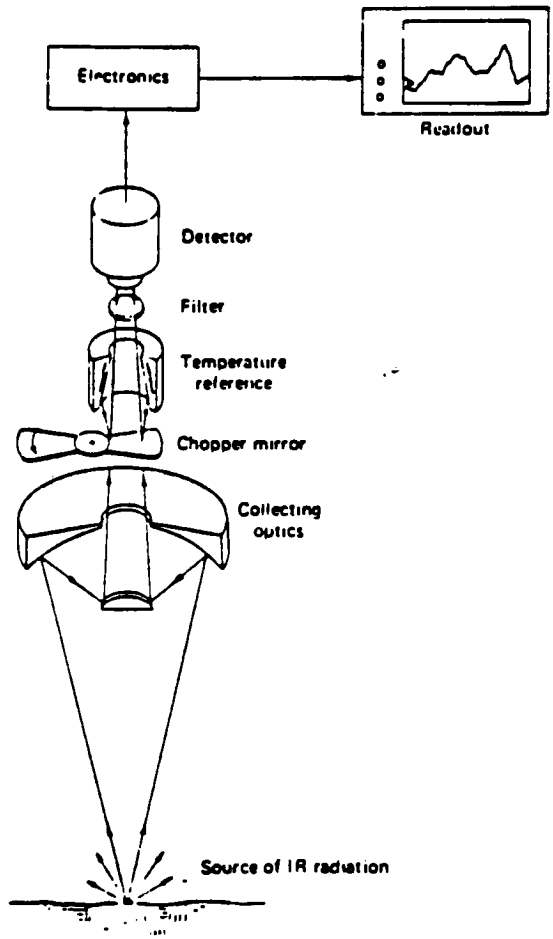

FIGURE 5: THERMAL RADIOMETER SCHEMATIC

after LILLESAND (1979)

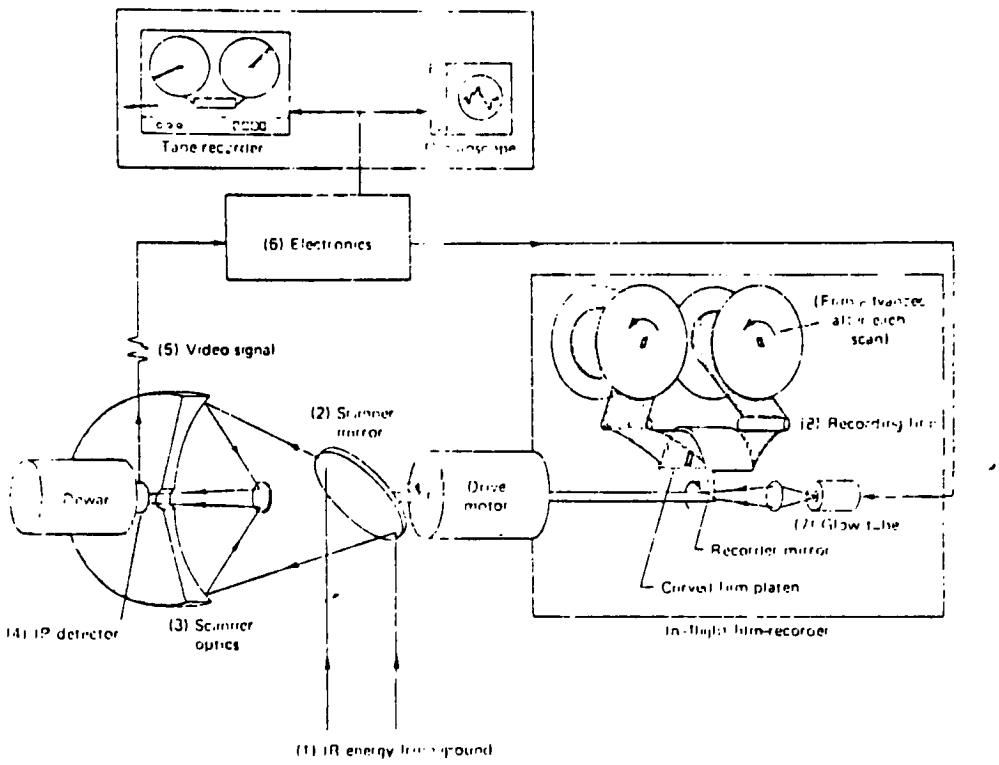

FIGURE 6: THERMAL SCANNER SCHEMATIC

after LILLESAND (1979)

angular velocity, the ground element Δx will get larger with increasing distance from the nadir. This results in image scale compression at points away from the nadir and the distortion is known as tangential scale distortion. It also has the effect of distorting linear features off the nadir into s-shaped curvatures as shown in Figure 8. For this study, only angles from the vertical must be determined accurately, not scale; and therefore tangential scale distortion was not corrected.

Referring to Figure 9, the film is curved to keep the glow modulator tube focused on the film over the entire scan.

$$y_p/y_{max} = \theta_p/\theta_{max} \tag{29}$$

$$\theta_p = y_p\theta_{max}/y_{max}$$

where θ_p = instantaneous view angle

y = distance on the image from the nadir line to point

y_{max} = distance from the nadir line to the edge of the image

θ_{max} = ½ the total view of the scanner

Equation 29 was used to determine the view angle for all targets measured in this study.

Other errors inherent in an airborne system are due to roll, pitch and yaw of the aircraft, but these can minimized with proper collection procedures.

A final error is introduced by improper velocity/height (v/h) settings. This error results in the scan lines being too close or too far apart which will compress or stretch the image along the flight line. The proper v/h settings are obtained from the calibration curves

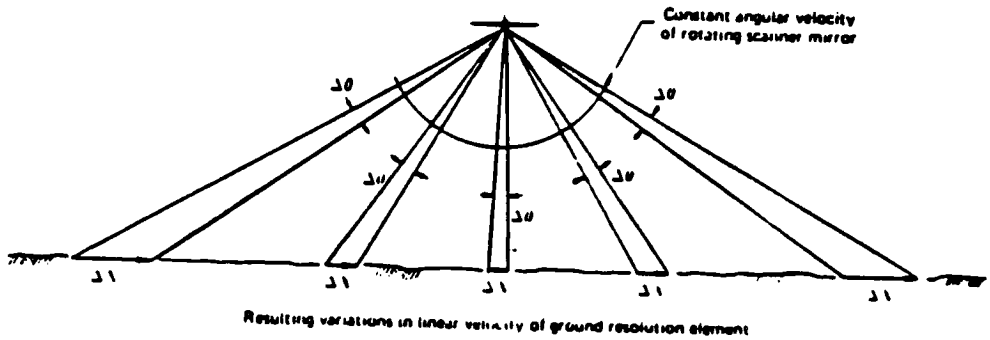

FIGURE 7: TANGENTIAL SCALE DISTORTION

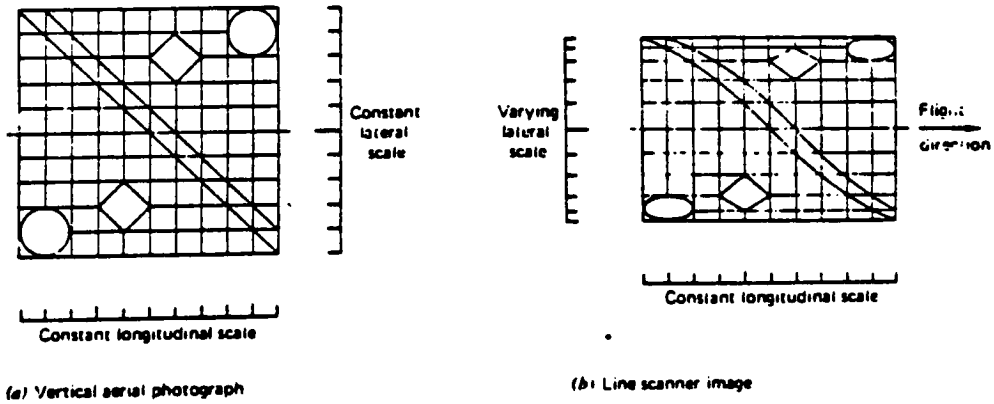

FIGURE 8: SCANNER IMAGE COMPRESSION

after LILLESAND (1979)

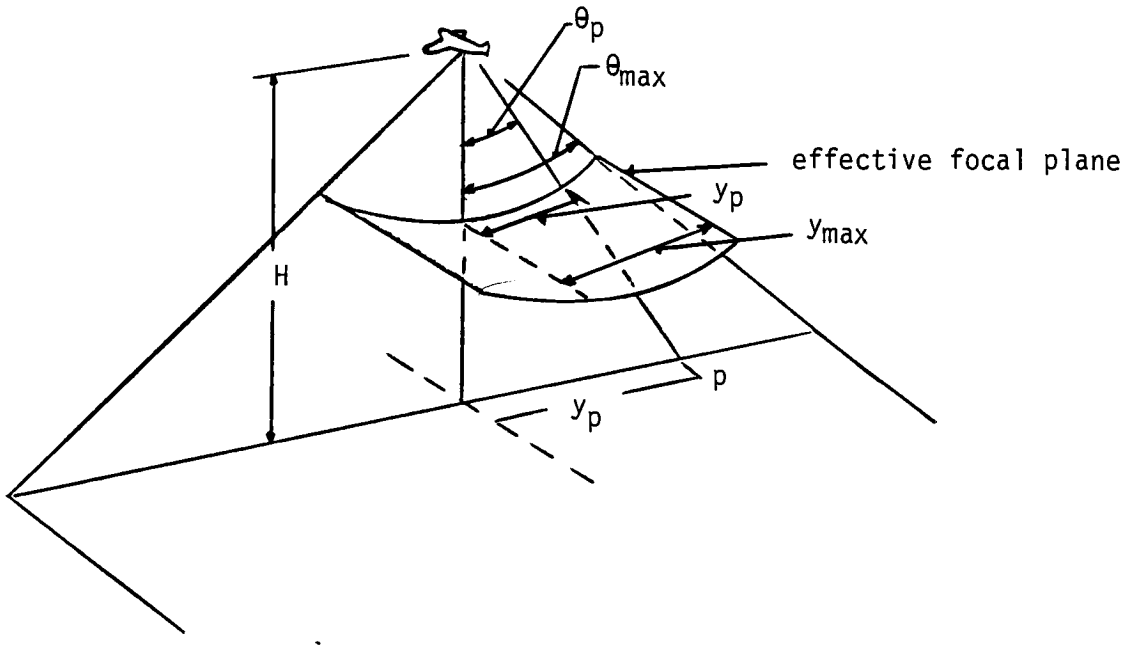

FIGURE 9: TANGENTIAL SCALE DISTORTION CORRECTION

after LILLESAND (1979)

as discussed under the subsection Calibrations of Sensors. The v/h settings only effect the image along the flight line; not transverse to it; and therefore did not produce any errors pertaining to this study.

3.3 Calibration of Senors

The approach to scanner calibration, used for this study involves several steps and is described here.

Initial calibration involves the use of a step wedge to give the relation between density produced on the film and voltage out of the detector. This curve is produced for each velocity/height (v/h) setting and an example is given in Figure 10.[18]

System linearity is then checked using water baths at different temperatures. Temperatures vs. voltage is plotted (Figure 11) with gain and DC level settings being held constant. This gives the conversion from output voltage through density to temperature at a particular gain setting and it should be linear in form.

Then the system gain is varied. The system gain is defined as the change in voltage associated with a unit change in temperature. This is carried out again by using water baths and the change in voltage over the change in bath temperature are plotted vs. gain setting (Figure 12).

The last step in scanner calibration involves using standard known temperatures modeled by blackbodies. Temperature controlled standards are used and the measured temperature can be set against the actual temperature through the blackbody settings as shown in Figure 13.

In summary for calibration:

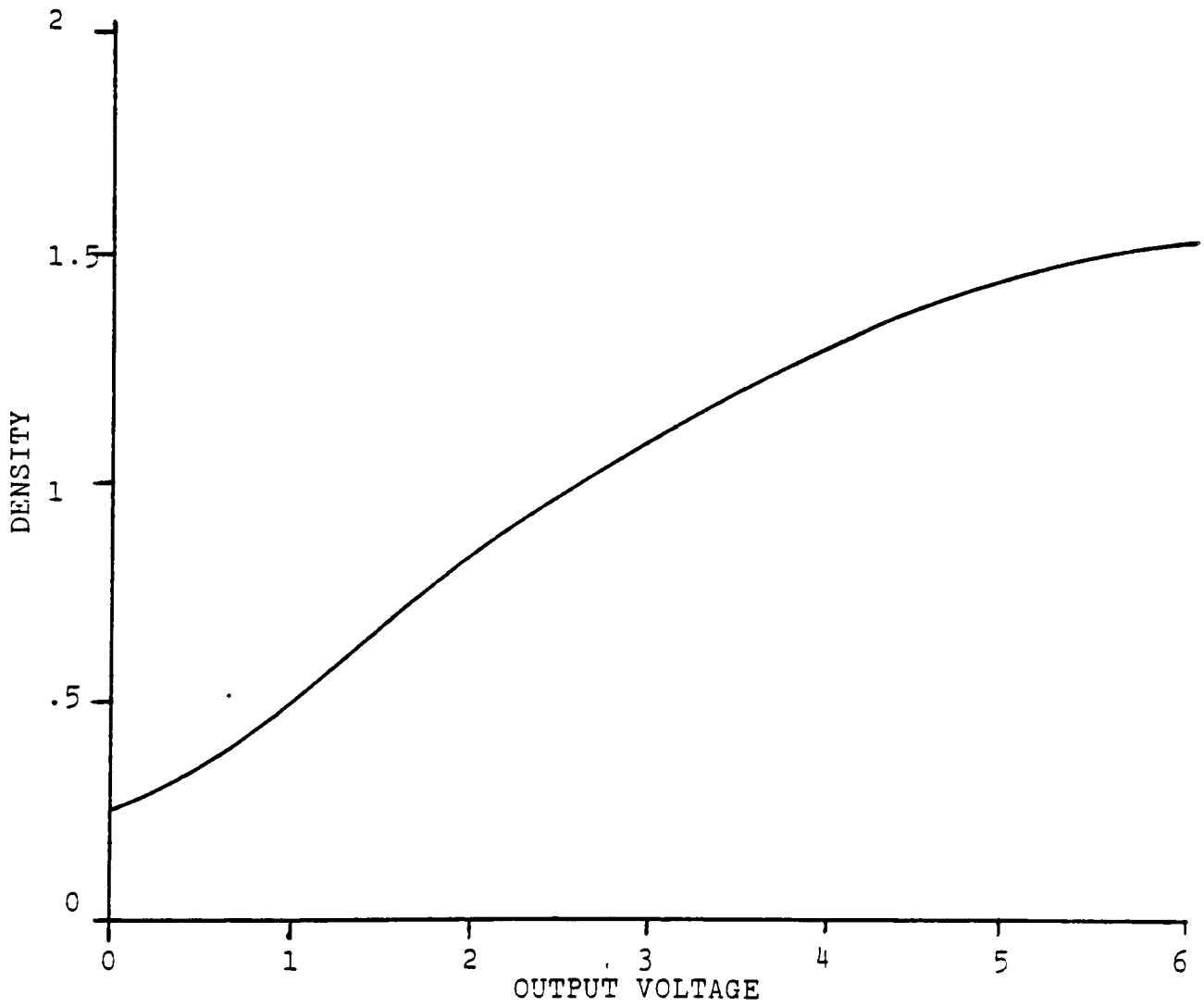

FIGURE 10

FILM-DENSITY Vs. SCANNER OUTPUT

after SCHOTT (19

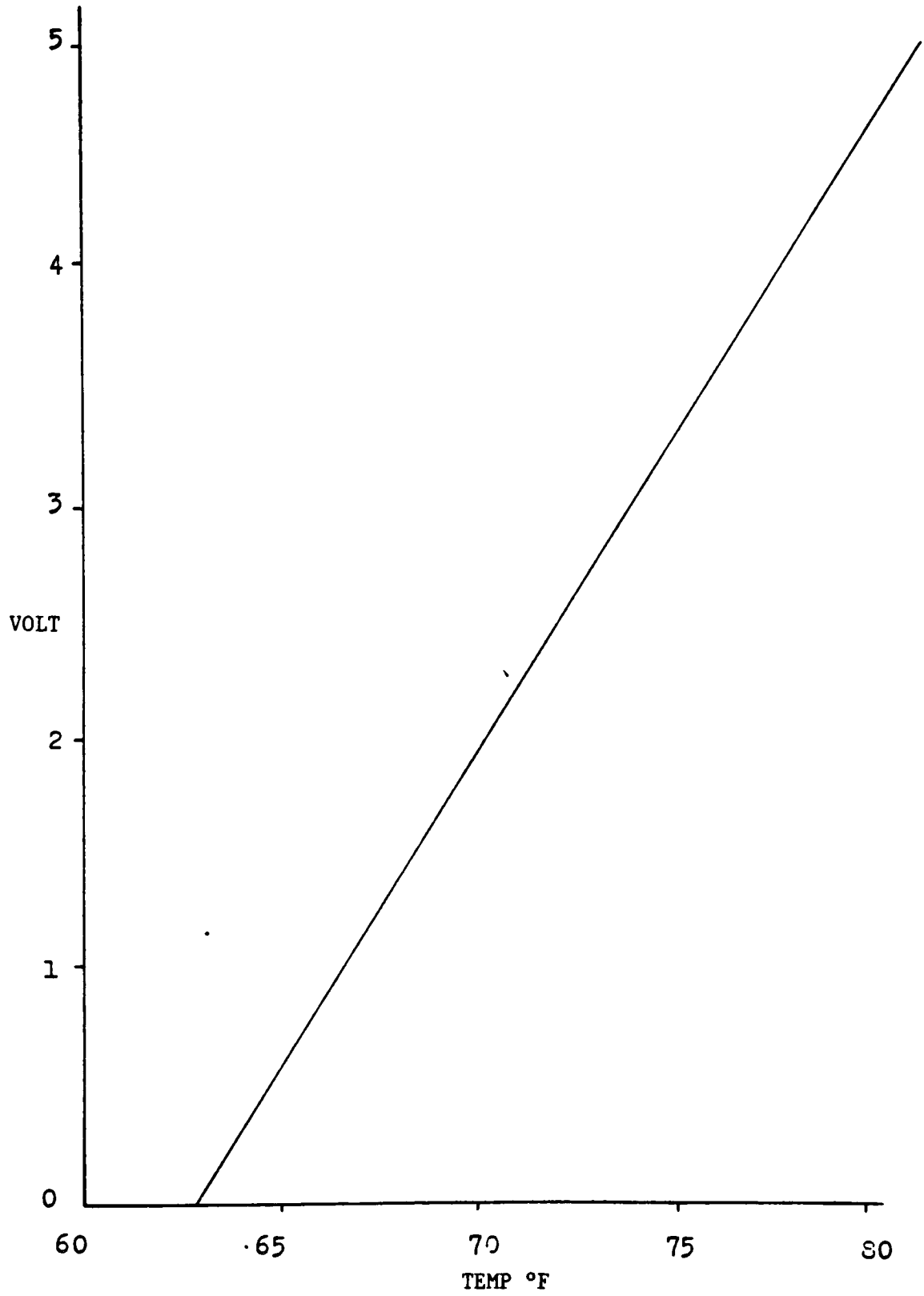

FIGURE 11
DETECTOR OUTPUT VOLTAGE VS. TEMPERATURE
AFTER SCHOTT (1976)

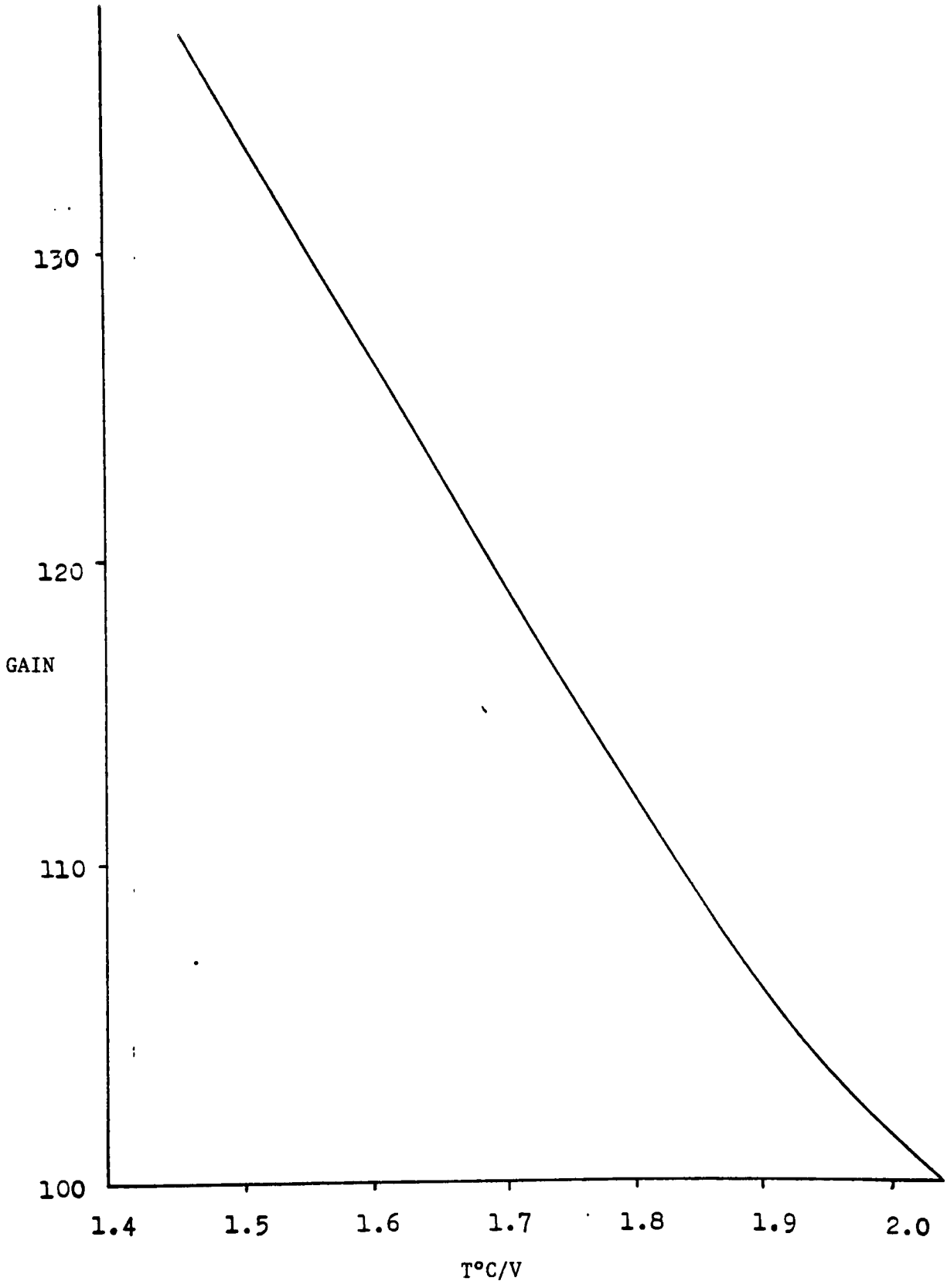

FIGURE 12
I.R. SCANNER GAIN VS. TEMP/VOLT
AFTER SCHOTT (1976)

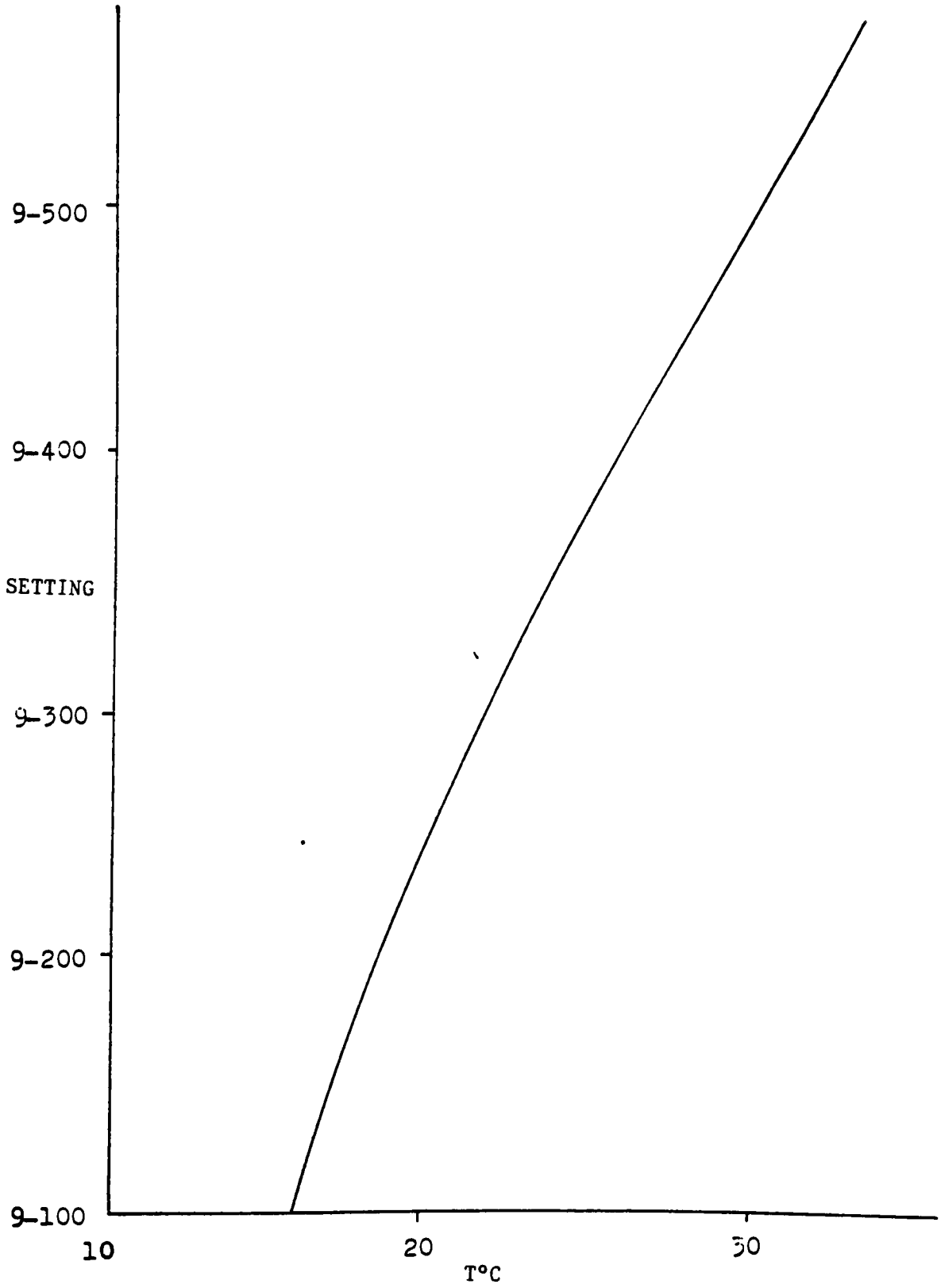

FIGURE 13
BLACKBODY CALIBRATION

$$V = gT + V_0 \tag{31}$$

where g = gain setting

V = output voltage

T = temperature

V_0 = initial voltage (intercept of response curve)

In Equation 31, V is obtained by reading the density of a blackbody calibration strip along the bottom edge of the imagery and converting this through the density-voltage step wedge (Figure 10). Given the gain setting and the blackbody temperature T then V_0 can be determined. Finally for an unknown temperature, density is measured, converted through a step wedge to V, and temperature is obtained using the gain and V_0 values previously calculated.

SECTION 4

EXPERIMENTAL

4.1 Experimental Method

A major assumption must be made for using Equation 25, in that the material being measured is Lambertian in character. This entailed carefully selection of the proper surface to be studied. Preliminary experimentation was carried out using a Barnes PRT-5 radiometer to measure various surfaces at different angles. Measurements were taken when the sky was clear and cold, compared to the surface, in order to minimize the background signal and give a true reading of only the surface. If the measured radiant energy did not vary significantly with different angles, then it was assumed that the material was nearly Lambertian in character. It is known for some materials that this is generally true within certain limits,[27,28,29] and the Lambertian assumption would hold over angles that are not extreme (0 ± 60°). These limits were adhered to for this study to determine the feasibility of this calibration technique.

Once the preliminary experimentation was completed, and the surfaces selected, the imagery was obtained. From the parameters given for the detector used, an error analysis was carried out to determine the theoretical error expected with this system. After data was taken, the error analysis was repeated with better estimtes of all the variables.

One of the necessary conditions for this technique to work was to have thermal imagery with parallel flight lines, of a set of objects. This is due to the fact that a regression would be carried out from measurements taken of a set of objects viewed vertically in one image and then the same set of objects in a separate image all offset by an equidistant amount (constant angle).

Considerable difficulty was encountered trying to obtain images with parallel flight lines. A point was reached when flight lines were transferred to a map in order to find a segment long enough to take a good number of sample points.

Densitometric measurements were then made of the surfaces at vertical angles and various offset angles. Also included for each film were densitometric measurements of the step wedge and the black body strip along the edge of the film (Figure 14). It was quickly discovered that many of the objects selected to be measured were very small. A 1 mm aperature was inserted in the Macbeth 101 densitometer but the diameter was too large for small objects like house rooftops because of the altitudes involved. Therefore a microdensitometer was used. The spot size was set to minimize the effect of picking up lines traced by the scanner as the images were made. The microdensitometer required calibration and this was done by matching readings of base plus fog and the upper end of the step wedge on the macrodensitometer with the microdensitometer.

As shown on the flow chart, (Figure 15), voltages were obtained from the density readings by a linear interpolation of the step wedge due to the fact that each density on the step wedge represented a one volt differential. From voltage, temperature was calculated using Equa-

FIGURE 14

Schematic Determination of $\tau(h,\phi)$ and $W_A(h,\phi)$

Vertical	Process	Angle
density		density
↓	step wedge	↓
voltage	$T = (V-V_0)/g$ (31)	voltage
↓		↓
temperature	Plancks (2)	temperature
$W(h,0)$		$W(h,\phi)$

regression

$$W(h,\phi) = mW(h,0) + b \quad (25)$$

$$m = \tau(h,0)^{(\sec\phi - 1)} \quad (26)$$

$$\tau(h,0)$$

$$\tau(h,\phi) = \tau(h,0)^{(\sec\phi)} \quad (19)$$

$$\tau(h,\phi)$$

$$b = (\sec\phi - m)W_A(h,0) \quad (28)$$

$$W_A(h,0)$$

$$W_A(h,\phi) = W_A(h,0)\sec\phi \quad (20)$$

$$W_A(h,\phi)$$

FIGURE 15

Schematic Determination of Apparent Temperature

Step	Method
density	
↓	step wedge
voltage	
↓	$T = (V-V_0)/g$ (31)
temperature	
↓	Plancks (2)
$W(h,\phi)$	
↓	
$W_0(0,\phi) = (W(h,\phi) - W_A(h,\phi))/\tau(h,\phi)$ (13)	
given $W_A(h,\phi)$, $\tau(h,\phi)$	
$W_T = (W_0(0,\phi) - W_S R(\phi)/\varepsilon(\phi)$ (14)	
given $W_S R(\phi)$, $\varepsilon(\phi)$)	
through Plancks equation	
apparent temperature	

tion 31. V_0 was first calculated using the density of the blackbody strip, interpolating through the step wedge to get voltage and again applying Equation 31 given the temperature of the blackbody and the gain.

From temperature, radiance was calculated using Plancks law but integrating over wavelength limits of 8-14 μm. This was accomplished by using Simpsons' rule and dividing the limits into twenty intervals. This method of using Simpsons' rule was checked against blackbody tables[29] and other double precision programs and this proved more than adequate.

With observed raidance determined, a regression was then carried out of $W(h,\Theta)$ versus $W(h,0)$, i.e.: radiance measured at altitude and at an angle versus radiance meaured vertically at altitude. Applying Equation 25, the slope and intercept were determined. As theoretically predicted $\tau(h,0)$ was obtained using Equation 26, and similarly $W_A(h,0)$ was obtained using Equation 28. Thus determination of atmospheric transmission and path radiance was possible.

In summary the process to obtain transmission and path radiance is shown schematically in Figure 14. The procedure for measurement of unknown temperature is outlined in Figure 15. The density is measured, converted to temperature and then radiance. The radiance value is then used as $W(h,\phi)$ for the general case and converted to W_T through Equations 13 and 14. Then apparent temperature can be calculated using Plancks equation.

4.2 Verification of Lambertian Assumption

Considerable equipment difficulties were encountered with the preliminary experimentation in trying to determine which surfaces were Lambertian. The problem was isolated to battery failure in the Barnes PRT 5 radiometer and this was eventually rectified. Measurements were then taken of the following objects.

1) water
2) soil
3) wood
4) asphalt
5) concrete
6) grass
7) brick

The results indicated that most man-made objects appear to be Lambertian in character, whereas natural surfaces were not. An example is shown in Table 1, with overall results listed in Appendix G.

TABLE 1

Lambertian Assumption Evaluation

Angle	Asphalt (V) (Lambertian)	Water (V) (Non-Lambertian)
0	0.18	0.20
10	0.18	0.14
20	0.18	0.14
30	0.18	0.16
40	0.18	0.20
50	0.18	0.20
60	0.18	0.19
70	0.20	0.19

The Lambertian character for man-made objects held up to 50° offset from the vertical. Therefore primarily man-made objects such as roads, house tops and factories were used as objects for this study.

4.3 Experimental Results

Thermal IR film from three separate flights was obtained from Calspan Corporation. The imagery was of Stirling (northern New York State), Plattsburgh (northwest New York) and Allentown (central Pennsylvania). Ambient temperature on all three flights was typical of a cold winter night; (between -10°C and 0°C); and the imagery appeared quite clear and high in resolution. Although many separate images were available, only one or two pairs per flight met the criteria of parallel flight lines within 5° over the length of measurement. This criteria was based on being as strict as possible but allowing enough leeway to utilize the imagery obtained.

Appendix A shows one set of data and all the conversions and is typical of all data obtained. Table 2 shows final results for all three flights. The results of this angular calibration are compared to data given for the same areas by Schott's (1977) multiple altitude extrapolation technique.[21] Schott's technique is included as Appendix I.

Based on the experimental results an error analysis was carried out. This statistically provided an estimate of the variability of the results. A full description of the method is described in Appendix H.

Table 3 shows a summary of the error analysis. Points were taken from each data set that were typical of the upper and lower boundaries of density to represent the full range of temperatures possible.

TABLE 2

Calibration Results

	Plattsburgh	Stirling	Allentown
n	53	32	90
R^2	0.99317	0.9989	0.99368
m	0.99448	0.97324	0.97051
b	6.268×10^{-5}	1.1077×10^{-4}	1.292×10^{4}
$\tau_1(h,0)$	0.9681	0.91898	0.9226
$WA_1(h,0)$	3.59×10^{-4}	3.164×10^{-4}	3.2254×10^{4}
$\tau_2(h,0)$	0.96316	0.92122	0.91935
$WA_2(h,0)$	6.3248×10^{-4}	2.893×10^{-4}	3.436×10^{-4}
ϕ	31.2	40.8	43.2

notes 1) $T_1(h,0)$, $WA_1(h,0)$ is by angular calibration

2) $T_2(h,0)$, $WA_2(h,0)$ is by multiple altitude extrapolation

3) n is the number of points

4) R^2 is the correlation coefficient

5) m is the slope

6) b is the Y axis intercept

TABLE 3

Error Analysis

Variable	Stirling	Platsburgh	Allentown
$\tau(h,0)$	0.918988	0.9681	0.922623
$W_A(h,0)$	0.000316	3.59×10^{-5}	0.000322
W_{T1}	0.002666	0.0027559	0.00266
W_{T2}	0.003924	0.003699	0.004208
W_{O1}	0.002501	0.002581	0.002495
W_{O2}	0.003604	0.00343	0.003889
$W_1(h,0)$	0.002614	0.00253	0.002624
$W_2(h,0)$	0.003655	0.003356	0.003910
ϕ	40.8	31.2	43.2
$\tau(h,\phi)$	0.89440	0.96247	0.895407
$W_A(h,\phi)$	0.0004174	4.197×10^{-5}	4.417×10^{-4}
$W_1(h,\phi)$	0.002654	0.002526	0.002676
$W_2(h,\phi)$	0.003667	0.003344	0.003924
m	0.97324	0.99448	0.970501
b	0.000108	6.268×10^{-5}	1.292×10^{-4}
S(m)	0.005629	0.0011545	0.008504
S(b)	2.579×10^{-6}	6.27×10^{-7}	2.591×10^{-6}
$S(W_A)$	1.3729×10^{-5}	3.811×10^{-6}	1.396×10^{-5}
$S(\tau)$	0.0167	0.0067	0.021
$S(W_O)$	4.9658×10^{-5}	2.1974×10^{-5}	6.238×10^{-5}
$S(W_T)$	7.306×10^{-5}	5.4997×10^{-5}	8.420×10^{-5}
S(temp)	0.4059	0.3055	0.4678

note: s(x) represents the error in the variable x. For example, s(temp) is the error in temperature.

SECTION 5

DISCUSSION

5.1 Analysis of Experimental Results

From Table 2 the angular calibration technique and multiple altitude extrapolation technique seemed to give consistent results. There is the question however of the reliability of the numbers. To validate this method, several tests were applied.

The first test carried out to verify accuracy consisted of checking the numbers of points taken. This was done on all three flights. Table 4 shows that 50 or more points were required to get stability in τ to 2 decimal places.

TABLE 4

τ Stability Based on Number of Points

N	Stirling	Platsburgh	Allentown
10	0.9334	0.82914	0.94183
20	0.9229	0.86243	0.92229
30	0.91898	0.89076	0.93306
40	--	0.90681	0.93436
50	--	0.96784	0.92128
60	--	--	0.92835
70	--	--	0.92261
80	--	--	0.92513
90	--	--	0.92262

It should be noted that the maximum number of points possible were taken with Stirling. Because of a limited number of Lambertian surfaces and a short image compared to the other two flights, only a total of 32 points were measured. However the results were still very consistent and were considered valid.

Table 5 shows a similar result to get W_A stable in only the first digit although W_A is a much smaller number than τ.

TABLE 5

W_A Stability Based on Number of Points

N	Stirling	Platsburgh	Allentown
10	2.678×10^{-4}	7.280×10^{-4}	2.459×10^{-4}
20	3.0809×10^{-4}	6.5212×10^{-4}	2.957×10^{-4}
30	3.164×10^{-4}	5.857×10^{-4}	2.6886×10^{-4}
40		5.262×10^{-4}	2.44175×10^{-4}
50		3.592×10^{-4}	3.0075×10^{-4}
60			3.0217×10^{-4}
70			3.125×10^{-4}
80			3.1344×10^{-4}
90			3.2254×10^{-4}

A second indication of the accuracy results from the regression itself. For all cases a correlation coefficient was calculated and it turned out to be above 99%, as shown in Table 2, indicating an excellent regression. This also verifies that a linear relationship does hold true for $W(h,\Theta)$ vs. $W(h,0)$. This is emphasized by Figures 14-16 where $W(h,\Theta)$ were plotted against $W(h,0)$ with error bars of $\pm$ 0.5°K included.

FIGURE 16

ANGULAR CALIBRATION-STIRLING-32 POINTS

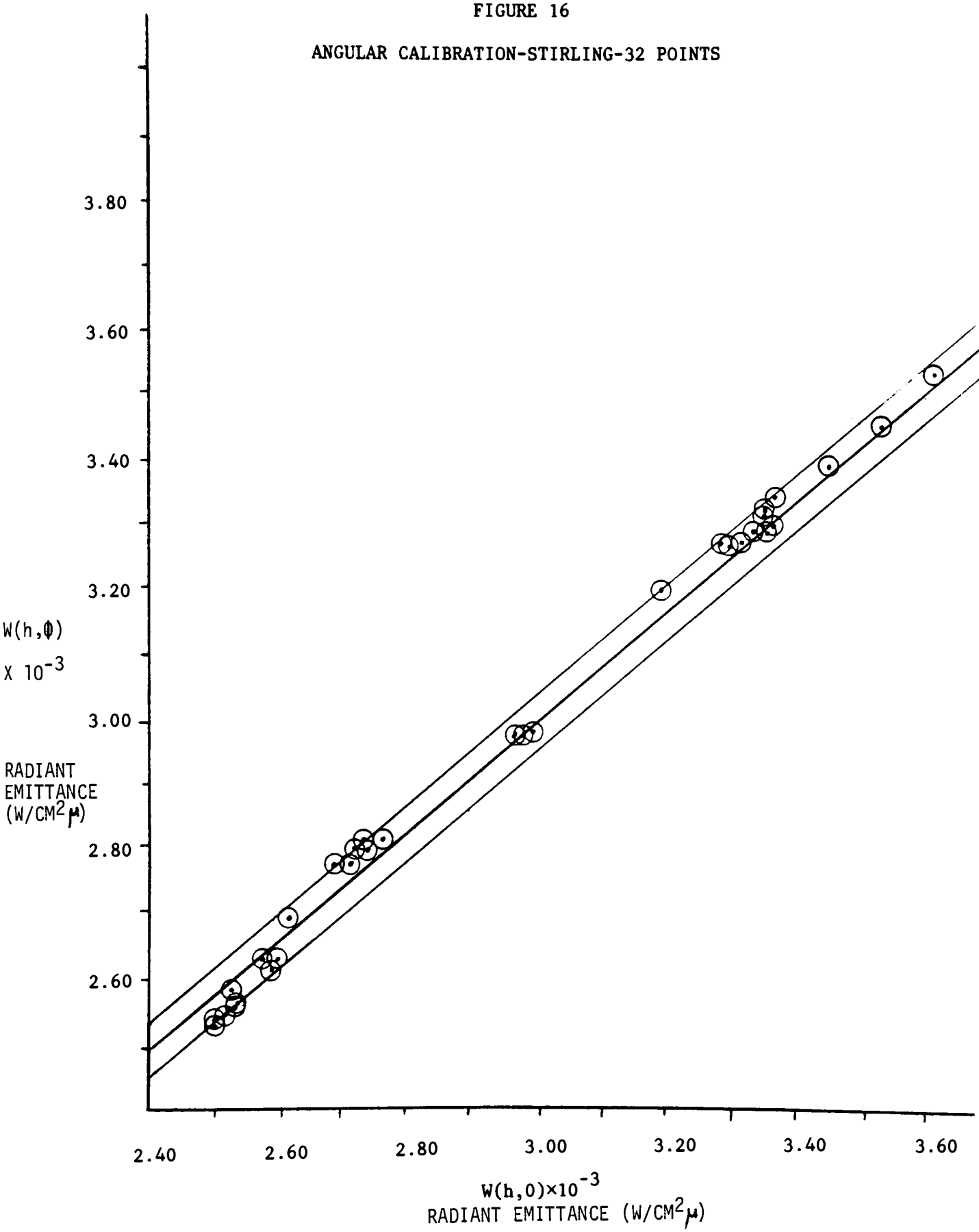

FIGURE 17

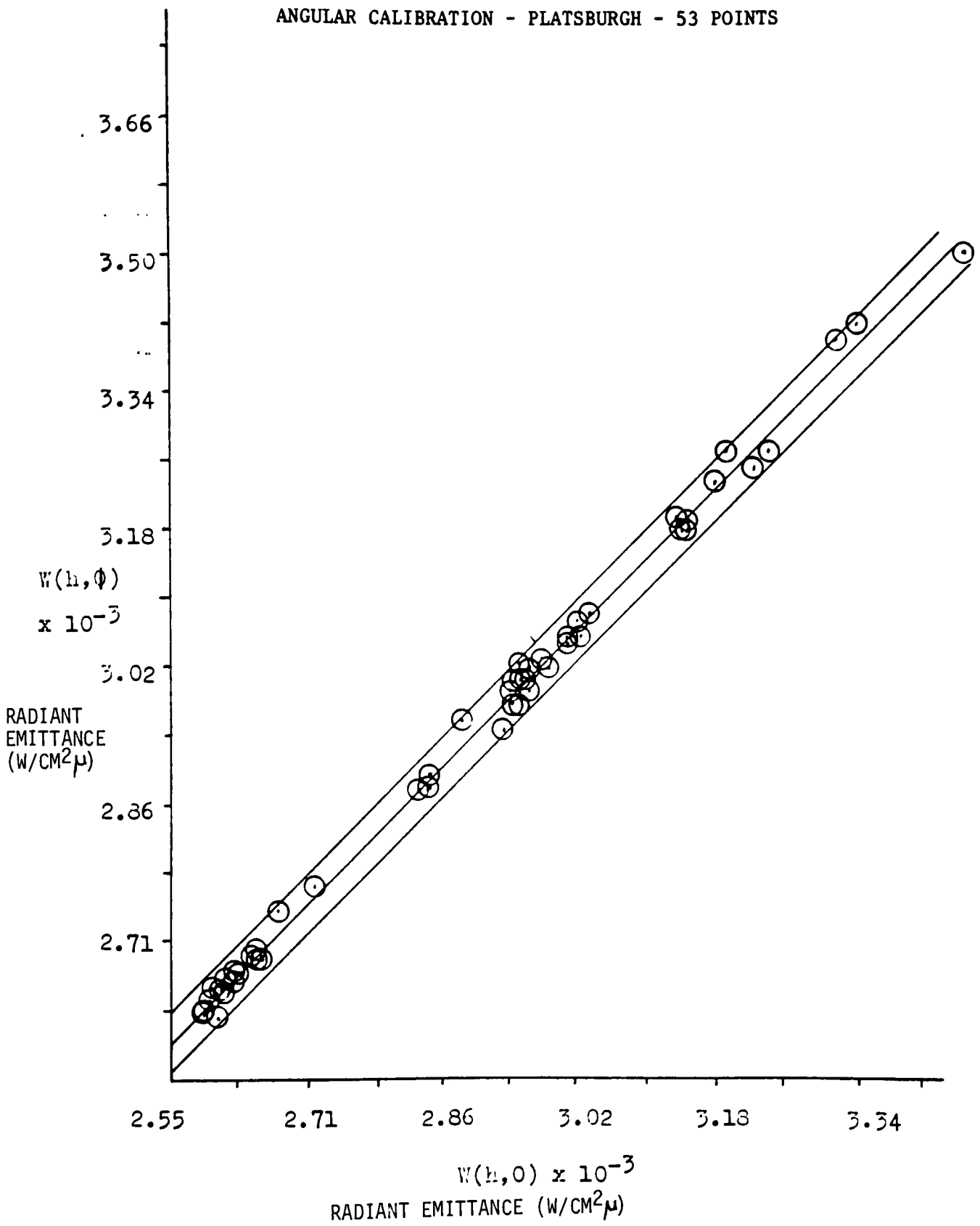
ANGULAR CALIBRATION - PLATSBURGH - 53 POINTS
3.66
3.50
3.34
3.18
3.02
2.86
2.71
W(h,Φ)
x 10⁻³
RADIANT
EMITTANCE
(W/CM²μ)
2.55
2.71
2.86
3.02
3.18
3.34
W(h,0) x 10⁻³
RADIANT EMITTANCE (W/CM²μ)

FIGURE 18

ANGULAR-CALIBRATION- ALLENTOWN - 90 POINTS

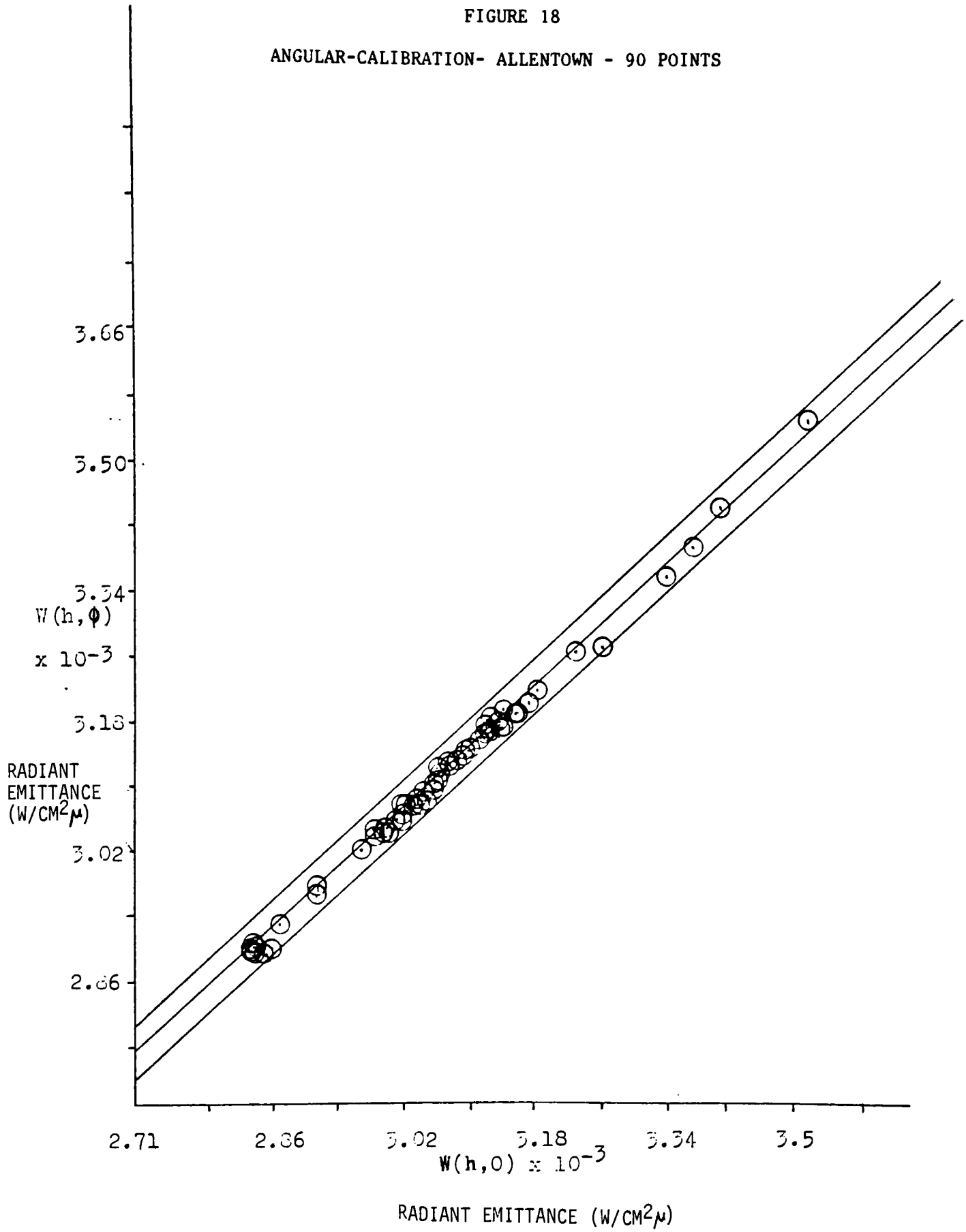

From the regression a confidence interval was placed on the slope and intercept parameters. This was based on using the students t distribution and involved the following formulae.[26]

$$m - \frac{t_{\delta/2} s}{\sqrt{SXX}} < m < m + \frac{t_{\delta/2} s}{\sqrt{SXX}} \tag{32}$$

$$b - \frac{t_{\delta/2} S\sqrt{\Sigma W(h,0)^2}}{\sqrt{nSXX}} < b < b + \frac{t_{\delta/2} S\sqrt{\Sigma W(h,0)^2}}{\sqrt{nSXX}} \tag{33}$$

where SXX = x sum of squares

S = standard deviation

m = slope

b = intercept

$t_{\delta/2}$ = value of t distribution at δ = 95% confidence level

n = number of points

For these equations a confidence level of 95% was chosen. If a higher confidence level was chosen the interval would have been wider thus improving the results even further. From the upper and lower limits on m a confidence interval on $\tau(h,0)$ was calculated using equation 26, and similarly a confidence interval on $W_A(h,0)$ was calculated using equation 28. The results are shown in Table 6. $\tau(h,0)$ for Platsburgh theoretically should not reach a value exceeding 1.0 but the statistical method does not recognize this for the confidence interval. All values are well within limits compared with the multiple altitude technique.

TABLE 6

Statistical Confidence Interval

		Lower Limit	Actual	Upper Limit	Multiple Altitude
Platsburgh	m	0.97210	0.99453	1.01095	-
	b	3.0168×10^{-6}	6.259×10^{-5}	1.2824×10^{-4}	-
	τ	0.8459	0.9681	1.1045	0.96316
	W_A	1.5543×10^{-5}	3.5856×10^{-4}	8.4290×10^{-4}	6.325×10^{-4}
Allentown	m	0.95678	0.973164	0.98954	-
	b	9.20514×10^{-5}	1.2109×10^{-4}	1.7013×10^{-4}	-
	τ	0.88797	0.92944	0.97114	0.91935
	W_A	1.7361×10^{-4}	3.0375×10^{-4}	4.4505×10^{-4}	3.436×10^{-4}
Stirling	m	0.96179	0.9732	0.9846	-
	b	7.6087×10^{-5}	1.098×10^{-4}	1.435×10^{-4}	-
	τ	0.8857	0.9189	0.9528	0.92122
	W_A	2.11809×10^{-4}	3.164×10^{-4}	4.2657×10^{-4}	2.893×10^{-4}

As another test, values of apparent temperature were calculated throughout the full density range of each film using τ and W_A obtained from both the angular technique and multiple altitude extrapolation technique, and then the apparent temperatures were compared. This was probably the most critical test as temperature is the ultimate goal of this system.

Tables 7, 8 and 9 illustrate the precision of apparent temperatures for each data set. The results show that if the angular techniques gave a lower τ value than the multiple altitude technique, then W_A turned out higher with the angular technique as compared to W_A from the multiple

TABLE 7

Comparison of Temperature - Stirling

D	Multiple Altitude τ = .92122 $W_A = 2.893\times10^{-3}$ Temp	Angular τ = .918988 $W_A = 3.164\times10^{-3}$ Temp	ΔT
.35	253.52	253.04	0.48
.40	254.77	254.3	0.47
.45	256.02	255.56	0.46
.50	257.27	256.82	0.45
.55	258.52	258.08	0.44
.60	259.76	259.33	0.43
.65	261	260.58	0.42
.70	262.24	261.83	0.41
.75	263.48	263.08	0.4
.80	264.72	264.33	0.39
.85	265.95	265.57	0.38
.90	267.18	266.81	0.37
.95	268.41	268.05	0.36
1.00	269.64	269.28	0.36
1.05	270.87	270.52	0.35
1.1	272.09	271.75	0.34
1.15	273.33	272.99	0.34
1.2	274.54	274.22	0.32
1.25	275.76	275.45	0.31
1.3	276.98	276.67	0.31
1.35	278.2	277.9	0.3
1.4	279.42	279.12	0.3
1.45	280.64	280.35	0.29
1.5	281.85	281.57	0.28
1.55	283.07	282.79	0.28
		$\Delta T(avg)$ =	0.37

TABLE 8

Comparison of Temperature - Platsburgh

D	Angular $\tau = .96781$ $W_A = 3.592 \times 10^{-5}$ Temp	Multiple Altitude $\tau = .96316$ $W_A = 6.3248 \times 10^{-5}$ Temp	ΔT
.45	259.07	258.79	0.28
.50	260.9	260.62	0.28
.55	262.73	262.46	0.27
.60	264.54	264.3	0.24
.65	266.36	266.13	0.23
.70	268.18	267.97	0.21
.75	270	269.8	0.2
.80	271.82	271.63	0.19
.85	273.64	273.47	0.17
.90	275.40	275.34	0.16
.95	277.28	277.13	0.15
1	279.1	278.96	0.14
1.05	280.92	280.79	0.13
1.1	282.74	282.62	0.12
1.15	284.56	284.45	0.11
		$\Delta T(avg)$	= 0.19

TABLE 9

Comparison of Temperature - Allentown

D	Angular $\tau = .922623_{-4}$ $W_A = 3.225 \times 10^{-4}$ Temp	Multiple Altitude $\tau = .919345_{-4}$ $W_A = 3.436 \times 10^{-4}$ Temp	ΔT
.45	251.95	251.45	0.5
.50	253.24	252.75	0.49
.55	254.53	254.06	0.47
.6	255.82	255.36	0.46
.65	257.11	256.66	0.45
.7	258.39	257.95	0.44
.75	259.67	259.25	0.42
.8	260.95	260.53	0.42
.85	262.23	261.82	0.41
.9	263.5	263.11	0.39
.95	264.77	264.39	0.38
1	266.04	265.67	0.37
1.05	267.31	266.94	0.37
1.1	268.57	268.22	0.35
1.15	269.84	269.49	0.35
1.2	271.1	270.76	0.34
1.25	272.36	272.03	0.33
1.3	273.61	273.3	0.31
1.35	274.87	274.57	0.3
		ΔT(avg) =	0.40

altitude technique. The overall result is an apparent temperature that is closely matching between the two different techniques. Assuming that the multiple altitude technique gave an exact temperature with no error the maximum error on temperature propogated experimentally by the angular technique was 0.5°C with the mean difference being 0.32°C. Given the error on the multiple altitude technique was 0.7°C,[21] this would produce an average root mean square error of 0.77°C, assuming that the errors on these two techniques were independent.

The next test consisted of purposely taking measurements off vertical from each pair of images but still maintaining parallel flight lines (i.e. the vertical and offset look angle were each displaced by the same amount). The data taken was from the Allentown flight with the 'vertical' measurements being offset 10° from vertical. This would mean that the vertical measurement was taken at 10° and the offset look angle measurement would be taken at 53.2 vice 43.2 from true vertical. Table 9 shows the results and when temperatures were again compared, the numbers were considered well within acceptable margins. A totally different set of objects was used for this test.

TABLE 10

Comparison of Vertical Offset and Normal Angular Calibration

	Offset	Normal
n	84	90
m	.971168	.970501
b	1.32116×10^{-4}	1.2944×10^{-4}
τ	.92432	.922623
W_A	3.2973×10^{-4}	3.2254×10^{-4}

At this time, unknown points were trialed. To fully test the system, objects like soil and water (known to not be Lambertian) were measured to determine if realistic temperatures would result. As expected, numbers that did not make sense could be explained by their non-Lambertian characters.

In summary, the following methods were used to evaluate the data:

1. comparison of $\tau(h,0)$ and $W_A(h,0)$ between angular calibration and multiple altitude extrapolation
2. varying number of points taken to check stability of $\tau(h,0)$ and $W_A(h,0)$
3. Correlation coefficient
4. Plots of $W(h,\phi)$ vs. $W(h,0)$ with error bars to verify linear relationship
5. Confidence interval on $\tau(h,0)$ and $W_A(h,0)$ based on statistical methods
6. Comparison of temperatures calculated by angular calibration and multiple altitude extrapolation
7. Offset vertical measurement from vertical and applying angular calibration
8. Entering unknown points
9. Error analysis

All of these methods led to the conclusion that the angular calibration technique developed in this study can be applied to correct for atmospheric effects. Assuming the multiple altitude extrapolation technique to be correct, experimental error in temperature proved to be a maximum of 0.5°C, whereas theoretical error predicted with typical numbers (error analysis) gave a maximum error of 0.46°C. It was found however that it was very difficult to stabilize $\tau(h,0)$ and $W_A(h,0)$ beyond two decimal places, even with a relatively high number of points

(90) because fluctuations in the extreme high and low density regions were very noticeable. This was apparent on the graphs of $W(h,\phi)$ vs. $W(h,0)$ where the error bars of ± 0.5°C just covered all points.

Offsetting the vertical measurements by ten degrees but maintaining the angle between measurements did little to change the value of $\tau(h,0)$ and $W_A(h,0)$ and this is further proof of the consistency of this method.

When applying this technique, it was noted that the maximum range possible in density (hence temperature) and the larger angles lead to the best results. This provided a wider base from which slope is calculated and produces less error. The angle was limited to the Lambertian limits set by the preliminary experimentation.

5.2 Path Radiance Assumption Evaluation

After some measurements were taken to get estimates of the variables, the path radiance assumption (Equation 20) was investigated further. The method involved calculating W_A propogated through the general case of an inhomogeneous atmosphere at a vertical angle, and comparing it to W_A calculated at various offset look angles. The goal here was to verify equation 20. Writing the general form of W_A incremented through many layers of atmosphere with W_A and τ changing from layer to layer gives:

$$W_A(h,0) = \int W_{Ai}/h \; \tau_i dh \tag{34}$$

where the subscript i refers to each atmospheric layer and τ_i is total transmittance to the point of observation. For various offset look angles τ changes by Beers' Law (Equation 19). This gives

$$W_A(h,\phi) = \int \frac{W_{Ai}}{h \cos \phi} \tau_i^{1/\cos \phi} \, dh \tag{35}$$

Taking the ratio produces:

$$\frac{W_A(h,\phi)}{W_A(h,0)} = \frac{\int (W_{Ai}/h \cos \phi) \, \tau_i^{1/\cos \phi} \, dh}{\int (W_{Ai}/h) \, \tau_i dh} \tag{36}$$

This ratio still deals with the case of an inhomogeneous atmosphere and because of this constraint W_i and τ_i could change in each layer considered. In effect W_i and τ_i are then functions of altitude and this prohibits taking the actual integral. To circumvent this problem the ratio of $W_A(h,\phi)/W_A(h,0)$ was taken for each layer. The first step taken was to write the incremental values.

$$\frac{W_A(h,\phi)_i}{W_A(h,0)_i} = \frac{(W_{Ai}/h \cos \phi) \, \Delta h \tau_i^{1/\cos \phi}}{(W_{Ai}/h) \, \Delta h \tau_i} = A \tag{37}$$

where A = constant

Taking the ratio for each layer allows the terms W_{Ai}/h and Δh to be cancelled giving:

$$\frac{W_A(h,\phi)_i}{W_A(h,0)_i} = \frac{\tau_i^{(1/\cos \phi - 1)}}{\cos \phi} = A \tag{38}$$

The value of A will change for each increment but the range of A throughout all altitude levels will be small. Therefore when taking the

sum of all the incremental values A can be taken out of the summation as a constant.

$$\Sigma W_A(h,\phi)_i = \Sigma W_A(h,0)_i A \tag{39}$$

$$\Sigma W_A(h,\phi)_i = A\Sigma W_A(h,0) \tag{40}$$

$$\frac{\Sigma W_A(h,\phi)_i}{\Sigma W_A(h,0)_i} = A = \frac{\tau_i(1/\cos\phi - 1)}{\cos\phi} \tag{41}$$

At this point incremental values of τ were taken ranging from .9 (representing ground level) to 1 (representing τ at altitude). Various angles were also tabulated within the limits used for this study. The results are shown in Table 11 with $\bar{A}$ being the averaged value of the ratio for all altitudes. For Table 11 altitude was taken from 0 to 100 feet in 1 foot increments.

TABLE 11

Evaluation of Path Radiance Assumption

ϕ	$\bar{A}$	sec ϕ	$\bar{A}$/sec ϕ
30	1.146	1.155	0.992
35	1.208	1.221	0.989
40	1.287	1.305	0.986
45	1.387	1.414	0.981
50	1.516	1.556	0.975
55	1.684	1.743	0.966
60	1.909	2.0	0.954

For this study angles did not exceed 45° and therefore the error on the assumption of $W_A(h,\phi) = W_A(h,0)/\cos\phi$ did not exceed 2%.

The error was investigated in further detail in that a value of .98 $W_A/\cos\phi$ vs. $W_A/\cos\phi$ was used for Equation 19 and this was inserted in the main program. It was discovered that the value of τ calculated by this method is totally independent of this assumption and therefore τ remained exactly the same. However W_A did increase by a slight margin. For the Stirling data it was 1.0757×10^{-3} as compared to 9.940×10^{-4}. This was considered a minimal change and it was concluded that the path radiance assumption was adequate for this study.

CONCLUSIONS

This study developed and verified an angular calibration technique based on a linear relationship between radiant emittance and atmospheric attenuation effects for Lambertian objects in the 8-14 μm spectral region. The experimental analysis of this totally airborne approach indicates that atmospheric effects can be predicted without ground truth or multiple altitude extrapolations.

RECOMMENDATIONS

Due to the constraint of parallel flights lines and a limited budget, imagery from only three flights was utilized. This reduced the available data base and could place some doubt on the accuracy. Also, only Lambertian (man made) objects were used for the calibration. It is recommended that research with respect to the Lambertian assumption and a larger data base could lead to increased accuracy in the technique or else point out it's limitations. Also, as outlined under Theoretical Development of Equations, the method can be carried further to determine W_S and ultimately W_T. Further research in this area could only be beneficial.

REFERENCES

1. Altman, H.J., in The Theory of Photographic Process, 4th ed., James, T.H., ed., Macmillan Pub., Co., Inc., New York, 1966.

2. Anson, A. in Neblette's Handbook of Photography and Reprography - Materials, Processes and Systems, 7th ed., Van Nostrand Reinhold Co., New York, 1977.

3. Barford, N.C., Experimental Measurements, Precision, Error and Truth, Addison Wesley Pub. Co. Inc., Mass., 1967.

4. Beers, Y., Introduction to the Theory of Error, Addison Wesley Pub. Co. Inc., Mass., 1957.

5. Boudreau, R.D., Correcting Airborne Scanning Infrared Radiometer Measurements for Atmospheric Effects, NASA TM-X-69940, 1972.

6. Carroll, J. P. and Cupery, K.N., "Object Measurement of Resolution in Film Image", Applied Optics, Vol. 10, No. 11, 1971.

7. Chapman, R.M., Howard, J.N. and Miller, E.A., Atmospheric Transmission of Infrared Summary Report, Ohio State University Research Foundation, on W44-099 eng. 400, 1949.

8. Chedin, A., Scott, N.A. and Berroir, A., "A Single-Channel, Double-Viewing Angle Method for Sea Surface Temperature Determination from Coincident METEOSTAT and TIROS-N Radiometric Measurements," Journal of Applied Meteorology, Vol. 21, April 1982.

9. Holtes, M.R., et al., Fundamentals of Infrared Technology, Macmillan Company, New York, 1962.

10. Hudson, R., Infrared Systems Engineering, John Wiley and Sons, New York, 1969.

11. Lillesand, T.M. and Kiefer, R.W., Remote Sensing and Image Interpretation, John Wiley and Sons, New York, 1977.

12. Lloyd, J.M., Thermal Imaging Systems, Plenum Press, New York, 1975.

13. Lorenz, D., "Temperature Measurements of Natural Surfaces using Infrared Radiometers", Applied Optics, Vol. 7, No. 9, 1968.

14. Marks, L.S., Standard Handbook for Mechanical Engineers, 7th ed., McGraw-Hill, New York, 1967.

15. McMillan, L.M., "Estimation of Sea Surface Temperatures from Two Infrared Window Measurements with Different Absorption", Journal of Geophysical Research, Vol. 80, No. 36, 1975.

16. Piech, K.R., Gaucher, D.W., and Schott, J.R., "Terrain Classification using Color Imagery", Photogrammetric Engineering and Remote Sensing, Vol. 43, No. 4, 1977.

17. Prabhakara, C., Dalu, G. and Kunde, V.G., "Estimation of Sea Surface Temperature from Remote Sensing in the 11-13 μm Window Region", Journal of Geophysical Research, Vol. 79, No. 33, 1974.

18. Randall, C.M., "IR Atmospheric Effects", Optical Engineering, Vol. 14, No. 1, 1975.

19. Saunders, P.M., "Aerial Measurements of Sea Surface Temperature in the Infrared", Journal of Geophysical Research, Vol. 72, 1967.

20. Scarpace, F.L., Madding, R.P., Green, T., "Scanning Thermal Plumes", Photogrammetric Engineering and Remote Sensing, Vol. 41, No. 10, 1975.

21. Schott, J.R., "Thermal Remote Sensing Calibration Techniques", Calspan Corp. Report NA-6019-M-1, 1977.

22. Schott, J.R., "The Blue to Green Reflectance Rates and Lake Water Quality", Photogrammetric Engineering and Remote Sensing, Vol. 44, No. 10, 1978.

23. Schott, J.R., "Temperature Measurement of Cooling Water Discharged from Power Plants", Photogrammetric Engineering and Remote Sensing, Vol. 45, No. 6, 1979.

24. Schott, J.R., "Data Use Investigation for Applications Explorer Mission A", Calspan Corp. Report 6175-M-1, 1981.

25. Smith, H., Applied Regression Analysis, John Wiley and Sons, New York, 1966.

26. Walpole, R.E. and Myers, R.H., Probability and Statistics for Engineers and Scientists, 2nd ed., Macmillan Pub. Co. Inc., New York, 1978.

27. Weiss, M., "Airborne Measurements of Earth Surface Temperature (Ocean and Land) in the 10-12 and 8-14 μm Regions", Applied Optics, Vol. 10, No. 6, 1971.

28. Wolfe, W.L., The Infrared Handbook, Environmental Research Institute of Michigan, Michigan, 1978.

29. Woodlief, T. Jr., SPSE Handbook of Photographic Sciences and Engineering, John Wiley and Sons, Inc., New York, 1973.

30. Zissir, G.J., Fundamentals of Infrared Techniques, Macmillan Company, New York, 1962.

31. Kodak Publication M-28. "Applied Infrared Photography", 1977.

32. Kodak Publication M-29. "Kodak Data for Aerial Photography", 4th ed., 1976.

33. Kodak Publication N-17. "Kodak Infrared Films", 1976.

Appendix A

Sample Run - Stirling

Stirling - Calibration Data

G = 5.4

TBB = 2.5

DBB = 1.20

VBB = 3.7833

V_0 = 3.27037

Step Wedge

Voltage	Density
0	.35
1	.59
2	.86
3	1.09
4	1.24
5	1.33
6	1.44
7	1.52

Stirling - Readings

#	Identification	D(h,0)	D(h,ϕ)
1	water	1.17	1.17
2	factory	.60	.63
3	road	1.03	1.04
4	white building	.36	.39
5	road	1.1	1.11
6	factory	1.02	1.04
7	arch building	.77	.80
8	arch building	.73	.78

Appendix A (continued)

#	Identification	D(h,0)	D(h,ϕ)
9	connection	.77	.80
10	irregular building	.37	.39
11	irregular building	.44	.47
12	irregular building	.44	.47
13	irregular building	.37	.40
14	fork in road	1.01	1.02
15	building	.54	.57
16	road	1.12	1.12
17	building	.56	.60
18	road	.99	1.02
19	first row house	.35	.38
20	third row house	.52	.57
21	road	1.05	1.06
22	white building	.47	.52
23	factory	.59	.62
24	parking lot	1.00	1.01
25	road	1.06	1.07
26	long building	.58	.61
27	white building	.35	.38
28	building	.42	.46
29	road	.91	.93
30	water	1.00	1.02
31	house	.37	.40
32	house	.43	.46

Stirling - Conversions

Density	Voltage	Temp	W
1.17	3.53	274.58	.00362
.60	1.037	261.1	.00229
.63	1.1781	261.7	.002829
1.03	2.739	270.29	.003335
1.04	2.783	270.53	.003352
.36	.0417	255.23	.002511
.39	.166	256.4	.002546
1.1	3.067	272.06	.003447
1.11	3.133	272.42	.003466
1.02	2.696	270.06	.003319
1.04	2.783	270.53	.003348
.77	1.66	264.5	.002973
.80	1.27	265.1	.003024
.73	1.519	263.7	.002944
.78	1.704	264.7	.003001
.77	1.66	264.5	.00298

Appendix A (continued)

Density	Voltage	Temp	W
.8	1.77	265.1	.003023
.37	.083	255.95	.002524
.39	.166	256.4	.002546
.44	.375	257.53	.002603
.47	.5	258.2	.002626
.37	.083	255.95	.002524
.4	.2083	256.63	.002559
1.01	2.652	269.82	.003304
1.02	2.696	270.06	.003319
.54	.2916	259.28	.002724
.57	.9166	260.45	.002769
1.12	3.2	272.78	.003491
.56	.875	260.23	.002750
.60	1.037	261.1	.002798
.99	2.565	269.25	.003275
1.02	2.696	270.00	.003323
.35	0	255.5	.002501
.38	.125	256.18	.002533
.52	.7083	254.33	.002699
.57	.916	260.45	.002769
1.05	2.826	270.76	.003364
1.06	2.869	270.99	.003380
.47	.5	258.2	.002622
.52	.7083	259.33	.00269
.59	1	260.9	.002785
.62	1.11	261.5	.00282
1.00	2.608	269.59	.003291
1.01	2.651	269.82	.003304
1.06	2.869	270.99	.003377
1.07	2.913	271.33	.00339
.58	.9583	260.68	.002616
.61	1.074	261.3	.00281
.35	0	255.5	.00250
.38	.125	256.18	.00254
.42	.2916	257.08	.00258
.46	.4583	257.98	.00263
.91	2.217	267.47	.00316
.93	2.2304	267.94	.00329
1.00	2.608	269.59	.03307
1.02	2.696	270.06	.00332
.37	.083	255.95	.00252
.40	.2083	256.63	.002559
.43	.33	257.3	.002594
.46	.4583	257.98	.002629

Stirling - Results

ΔT	19.08
n	32
$\Sigma W(h,0)$	.09386
$\Sigma W(h,0)^2$	.0002786
$\Sigma W(h,\phi)$	.09485
$\Sigma W(h,0)W(h,\phi)$	.0002826
SXX	4.037×10^{-5}
SYY	3.8227×10^{-5}
SXY	3.934×10^{-5}
RSS	3.838×10^{-8}
SSR	3.839×10^{-5}
S^2	1.368×10^{-9}
R^2	.9989
m	.9732
S(m)	.00563
b	.0001098
S(b)	2.579×10^{-6}
ϕ	40.8
$\tau(h,0)$	.9189
WA(h,0)	.0003164
$\tau(h,\phi)$	.90377
WA(h,ϕ)	.0003934

Appendix B

Facilities and Equipment

Densitometers

Macbeth TD504; Serial # 892

Mcabeth 101; Serial # 801120

Microdensitometer

PMT EMT Emi. Genco Inc. B289F 1090

Bausch & Lomb fiber optic light source 33-32-20; Serial # 200078

Kepes Regulated DC Supply; Serial # 126312

Micro base Model LB-710 Richards

Calspan generated imagery

Light table

Barnes PRT 5 radiometer

Multimeter T lube 8022B

Atari Basic Computer 32K

Tripod

Appendix C

Main Program

```
5       PRINT "<ESC CONTROL CLR>"
6       PRINT "<CONTROL TAB> THESIS DATA CRUNCH"
10      PRINT "<CONTROL TAB> ____________________"
11      PRINT "NEW CALIBRATION DATA"
12      DIM F$(3), D1(8), V1(8)
13      INPUT F$:IF F$(1,1) = "Y" THEN 1500
14      READ G1,TBB,DBB
15      G = 1/G1:PRINT
16      PRINT "CURRENT CALIBRATION IS AS FOLLOWS:":PRINT
17      PRINT "V", "D":PRINT "__", "__"
18      FOR Z=0 TO 7
19      READ V1, D1:V1(Z)=V1:D1(Z)=D1
20      PRINT V1(Z), D1(Z)
21      NEXT Z
22      PRINT
23      DATA 2.5,-3.6,.84
24      DATA 0,.42,1,.49,2,.57,3,.66,Y,.78,5,.86,6,.92,7,.98
25      PRINT "G=, G1:PRINT "TBB=", TBB:PRINT "DBB=", DBB:GOSUB 1600
26      VO=VBB-(G*TBB)
27      PRINT "VBB=", VBB:PRINT "Vo=",VO
28      PRINT
40      PRINT "HOW MANY POINTS WERE TAKEN":INPUT P
42      DIM VV(P), VL(P), TV(P), TL(P), DV(P), DL(P)
43      PRINT
45      PRINT "INPUT DATA POINTS"
46      FOR X=1 TO P
47      PRINT "DV("; X; ")";:INPUT DV:DV(X)=DV
48      PRINT "DL(";X;")";:INPUT DL:DL(X)=DL
49      PRINT
50      NEXT X
51      PRINT
52      PRINT "DENSITY","VOLTAGE":PRINT "_____","_____"
53      FOR P2=1 TO P
54      X=1
55      IF D1(X) < DV(P2) THEN 70
56      VV(P2)=V1(X-1)+(((V1(X)-V1(X-1)*(DV(P2)-D1(X-1)))/
        (D1(X)-D1(X-1)))
57      X=1
58      IF D1(X) < DL(P2) THEN 65
59      VL(P2)=V1(X-1)+(((V(X)-V1(X-1))*(DV(P2)-D1(X-1)))/
        (D1(X)-D1(X-1)))
60      GOTO 71
65      X=X+1:GOTO 58
70      X=X+1:GOTO 55
71      PRINT DV(P2),VV(P2)
72      PRINT DL(P2),VL(P2)
73      PRINT
74      NEXT P2
75      PRINT
```

Appendix C (continued)

```
76      PRINT "PRESS ANY KEY TO CONTINUE"
77      PRINT "THE NEXT STEP IS CONVERSION TO TEMP"
78      OPEN #1,4,0,"K:":GET #1,T:CLOSE #1
79      PRINT "<ESC CONTROL CLR>"
80      PRINT "TV", "TL"
85      PRINT "___", "___"
90      FOR X=1 TO P
95      TV(X)=((VV(X)-V0)/G) + 273.16
100     TL(X)=((VL(X)-V0)/G) + 273.16
105     PRINT TV(X),TL(X)
110     NEXT X
115     PRINT "PRESS ANY KEY TO CONTINUE"
120     PRINT "THE NEXT STEP IS SIMPSONS"
125     PRINT "INTEGRATION"
130     OPEN #1,4,0,"K:":GET #1,T:CLOSE #1
131     PRINT "<ESC CONTROL CLR>":PRINT "<CONTROL TAB>
        SIMPSONS INTEGRATION":PRINT" <CONTROL TAB>
        "                      "
        ______________________
132     PRINT:PRINT:PRINT "WV","WL":PRINT "___", "___"
133     DIM W(P,2)
134     FOR X=1 TO P
135     FOR Q=1 TO 2
136     IF Q=1 THEN T=TV(X)
137     IF Q=2 THEN T=TL(X)
138     B=14:A=8
139     W1=(B-A)/20
140     W=A
155     GOSUB 350
160     Y1=F
165     W=B
170     GOSUB 350
175     Y2=F
180     C=0
185     D=0
189     REM LOOP FOR EACH INTERVAL
190     FOR I=1 TO (B-A)/W1-0.5
240     W=A+I*W1
242     GOSUB 350
244     Y=F
249     REM INTERVAL EVEN OR ODD
250     T2=I/2:R=INT(T2)
255     IF T2=R THEN 280
259     REM SUM ALL ODD INTERVAL FUNCTION VALUES
260     C=C+4
270     GOTO 290
279     REM SUM ALL EVEN INTERVAL VALUES
280     D=D+4
290     NEXT I
299     REM COMPUTE INTEGRAL
300     W(X,Q)-W1/3*(Y1+(C*4)+D*2+Y2)
310     PRINT W(X,Q)
```

Appendix C (continued)

```
320     GOTO 400
330     REM DEFINE FUNCTION
350     K=37415/π
360     L=14387.9
370     U=L/(W*T)
380     F=(K/(W^5))*(1/(EXP(U)-1))
390     RETURN
400     NEXT Q
410     PRINT
420     NEXT X
430     FOR S1=1 TO 3:PRINT "<ESC CONTROL 2>":NEXT S1
440     PRINT "PRESS ANY KEY TO CONTINUE"
450     PRINT "THE NEXT STEP IS THE REGRESSION"
460     OPEN #1,4,0,"K:":GET #1,T:CLOSE #1
470     PRINT "<ESC CONTROL CLR>"
471     PRINT "<CONTROL TAB>REGRESSION":PRINT "<CONTROL TAB>_____"
474     PRINT:PRINT
500     A=0:B=0:C=0:D=0:E=0:F=0:G=0:H=0:I=0:J=0:K=0:L=0:M=0:N=0:N=0:Q=0:
        S=0
510     FOR Z=1 TO P
520     A=A+W(Z,1)
530     B=B+W(Z,2)
540     C=C+1
550     D=W(Z,1)^2
560     E=E+D
570     F=W(Z,2)^2
580     G=G+F
590     H=H+(W(Z,1)*W(Z,2))
600     NEXT Z
610     I=((H*C)-(A*B))/(C*E-A^2)
620     J=B/C-I*(A/C)
630     K=E-(A^2/C)
640     L=G-(B^2/C)
650     M=H-(A*B/C)
660     N=L-(I*M)
670     Q=I*M
680     R=N/(C-2)
690     S=M^2/(K*L)
700     PRINT "N", C
710     PRINT "SUM WV",A
720     PRINT "SUM WV^2",E
730     PRINT "SUM WL",B
740     PRINT "SUM WV*WL",H
760     PRINT "SXX",K
770     PRINT "SYY(SST)",L
780     PRINT "SXY",M
790     PRINT "RSS",N
800     PRINT "SSR",Q
810     PRINT "S^2",R
820     PRINT
830     PRINT "R^2",S
```

Appendix C (continued)

```
840    PRINT
850    PRINT "M",I
860    PRINT
870    PRINT "b",J
880    PRINT "WL=";I;"WV+";J
890    PRINT
891    FOR Z=1 TO P
892    SX=((W(Z,1)-(A/P))^2)+SX
893    NEXT Z
894    SIG=SQR(R)
895    SB=(SQR(E/(P*SC)))*SIG
896    PRINT "S(B)=",SB
897    SM=SIG/(SQR(SX))
898    PRINT "S(M)=",SM
899    DEG
900    PRINT "INPUT ANGLE";:INPUT A:PRINT
910    TV=I^(1/COS(A)-1))
920    WAV=J/(1/COS(A)-I)
930    PRINT "TV=",TV
940    PRINT "WAV=",WAV
950    PRINT "WV="; TV; "WO+"; WAV
960    PRINT
970    TL=TV^(1/COS(A))
980    WAL=WAV/COS(A)
990    PRINT "WL="; TL; "Wo+"; WAL
995    PRINT
1000   PRINT "THATS ALL FOLKS"
1010   END
1500   PRINT
1505   PRINT "INPUT GAIN";:INPUT G1:G=1/G1
1510   PRINT "INPUT TBB IN CESIUS";:INPUT TBB
1515   PRINT "INPUT DBB"; INPUT DBB
1530   PRINT "INPUT DENSITY VALUES FOR STEP WEDGE"
1531   PRINT
1535   FOR Z=0 TO 7
1540   PRINT "DENSITY AT STEP #";Z;:INPUT D:D1(Z)=D
1541   V1(Z)=Z
1545   NEXT Z
1550   PRINT
1551   GOSUB 1600
1556   PRINT
1557   PRINT "VBB=";VBB
1558   VO=VBB-(G*TBB)
1559   PRINT "Vo="VO
1560   PRINT
1565   GOTO 40
1600   X=1
1610   IF D1(X)<DBB THEN 1670
1615   VBB=V1(Z-1)+(((V1(X)(-V1(X-1))*(DBB-D1(X-1)))/(D1(X)-D1(X-1)))
1620   RETURN
1670   X=X+1
1680   GOTO 1610
```

Appendix D

Error Analysis Program

```
10      PRINT "<ESC CONTROL CLR>"
20      PRINT "<CONTROL TAB> ERROR ANALYSIS"
25      PRINT "<CONTROL TAB>_____"
30      PRINT:PRINT
35      DEG
40      E=0.9:R=1-E
45      PRINT "ENTER T";:INPUT T
50      PRINT "ENTER WA";:INPUT WA
55      PRINT "ENTER WT1";:INPUT WT
60      WS=3.2E03/π
70      SR=0.015:SE=0.015
80      SWS=5.09E-05
85      SWL=1.14E-05:SWV=1.14E-05
90      WO=E*WT+R*WS
92      PRINT "ENTER WT2";:INPUT WT2:SL=.005
94      PRINT "ENTER S(M),S(B)";:INPUT SM, SB
95      PRINT "ENTER ANGLE;:INPUT L
96      PRINT "ESC<CONTROL CLR>"
97      PRINT "WO1=";WO
100     GOSUB 200
110     A=(1/E)Λ2*(SWOΛ2)
120     B1=(WJ/E)Λ2*(SRΛ2)
130     C=(R/E)Λ2*(SWSΛ2)
140     D=((WO-R*WS)/(EΛ2))Λ2*(SEΛ2)
150     SWT=SQR (A+B1+C+D)
160     PRINT "S(WT)=",SWT
170     STE=SWT/1.8E-04
180     PRINT "S(TEMP)=",STE
190     END
200     GOSUB 500
220     G=((WV-WA)/TΛ2))Λ2*(STΛ2)
230     H=(1/T)Λ2*(SWAΛ2)
235     F=(1/T)Λ2*(SWVΛ2)
240     SWO=SQR(F+G+H)
250     PRINT "S(WO)=",SWO
260     RETURN
500     WO2=E*WT2+R*WS
505     PRINT "WO2=,WO2
510     WV2=T*WO2+WA
515     WV=T*WO+WA
517     PRINT "WV1=",WV
518     PRINT "WV2=",WV2
520     TL=TΛ(1/COS(L))
521     WAL=WA/(COS(L))
522     PRINT "WAL=",WAL
523     PRINT "TL=",TL
525     WL2=TL*WO2+WAL
530     WL=TL*WO+WAL
540     M=(WL2-WL)/(WV2-WV)
```

Appendix D (continued)

```
545     PRINT "WL1=",WL
546     PRINT "WL2=",WL2
590     PRINT "M=",M
591     PRINT "S(M)=",SM
600     B=WL-(M*WV)
620     PRINT "b=",B
630     PRINT "S(b)=",SB
700     K=(1/COS(L))-M
710     N=(B*SIN(L))/((K^2)*(COS(L)^2))
720     SWA=SQR((((1/K)^2)*(SB^2))+(((B/(K^2))^2)*(SM^2))+(N^2)*(SL^2))
740     PRINT "WA=",WA
750     PRINT "S(WA)=",SWA
760     KV=(1/COS(L))-1
770     KS=(1/KV)*(M^(1/KV-1))
790     TP=(M^(KV^-1))*(KV^-2)*(COS(L)^-2)*SIN(L)*LOG(M)
800     ST=SQR((KS^2)*(SM^2)+(TP^2)*(SL^2))
810     PRINT "S(T)=",ST
820     RETURN
```

Appendix E

Conversion of D to TEMP Given T,WA
D Ranging From .35 to 1.5

```
5       PRINT "<ESC CONTROL CLR>"
6       PRINT "<CONTROL TAB> MULTIPLE DENSITY CONVERSION"
7       PRINT "<CONTROL TAB>_____________________"
10      PRINT
12      DIM D1(8),V1(8),F1(13)
14      READ G1,TBB,DBB
15      G=1/G1
16      PRINT:PRINT "CURRENT CALIBRATIONS IS AS FOLLOWS:":PRINT
17      PRINT "V", "D":PRINT "___", "___"
18      FOR Z=0 TO 7
19      READ V1, D1:V1(Z)=V1:D1(Z)=D
20      PRINT V1(Z),D1(Z)
21      NEXT Z
22      PRINT
23      DATA 2.5,-3.6,.94
24      DATA 0,.43,1,.63,2,.80,3,.94,4,1.09,5,1.20,6,1.30,7,1.38
25      PRINT "G=";G1:PRINT "TBB=";TBB:PRINT "DBB=";DBB:GOSUB 1600
26      VO=VBB-(G*TBB)
27      PRINT "VBB=";VBB:PRINT "Vo=";VO
28      PRINT
30      PRINT "ENTER T,WA";INPUT TL,WA
35      PRINT "ENTER ANGLE"; INPUT AN
40      PRINT
45      PRINT "D", "T", "WO":PRINT "___", "___", "___"
50      DE=.35
54      X=1
55      IF D1(X)<DE THEN 70
56      W=V1(X-1)+(((V1(X)-V1(X-1))*(DE-D1(X-1)))/(D1(X)-D1(X-1)))
60      GOTO 75
70      X=X+1:GO TO 55
75      T=((VV-VO)/G)+273.16:GOSUB 140
80      WO=(Z-(WA/COS(AN)))/(TL^(1)/COS(AN)))
122     DEG
124     T=270
130     GOTO 400
140     B=14,A=8
142     W1=(B-A)/20
144     W=A
155     GOSUB 350
160     Y=F
165     W=B
170     GOSUB 350
175     Y2=F
180     C=0
185     D=0
189     REM LOOP FOR EACH INTERVAL
190     FOR I=1 TO (B-A)/W1-0.5
240     W=A+I*W1
```

Appendix E (continued)

```
242   GOSUB 350
244   Y=F
249   REM INTERVAL EVEN OR ODD
250   T2=I/2:R=INT(T2)
255   IF T2=R THEN 280
259   REM SUM ALL ODD INTERVAL FUNCTION VALUES
260   C=C+4
270   GOTO 290
279   REM SUM ALL EVEN INTERVAL VALUES
280   D=D+Y
290   NEXT I
299   REM COMPUTE INTEGRAL
300   Z=W1/3*(Y1+(C*4)+D*2+Y2)
320   RETURN
330   REM DEFINE FUNCTION
350   K=37415/π
360   L=14387.5
370   U=L/(W*T)
380   F=(K/W^5))*(1/(EXP(U)-1))
390   RETURN
400   GOSUB 140
410   IF Z<WO THEN 430
420   T=T-1:GOSUB 140
425   GOTO 410
430   IF Z>WO THEN 450
440   T=T+0.4:GOSUB 140
445   GOTO 430
450   IF WO>Z THEN 470
460   T=T-0.1:GOSUB 140
465   GOTO 450
470   IF ABS(WO-Z)<2E-06 THEN 510
480   T=T+0.01:GOSUB 140
490   GOTO 470
510   PRINT DE,T,Z
520   DE=DE+0.05
525   IF DE>=1.6 THEN 1700
530   GOTO 54
1600  X=1
1610  IF D1(X)<DBB THEN 1670
1615  VBB=(V1(X-1)+(((V1(X)-V1(X-1))*(DBB-D1(X-1)))/D1(X)-D1(X-1)))
1620  RETURN
1670  X=X+1
1680  GOTO 1610
1700  FOR S1=1 TO 3:PRINT "<ESC CONTRL 2>":NEXT S1
```

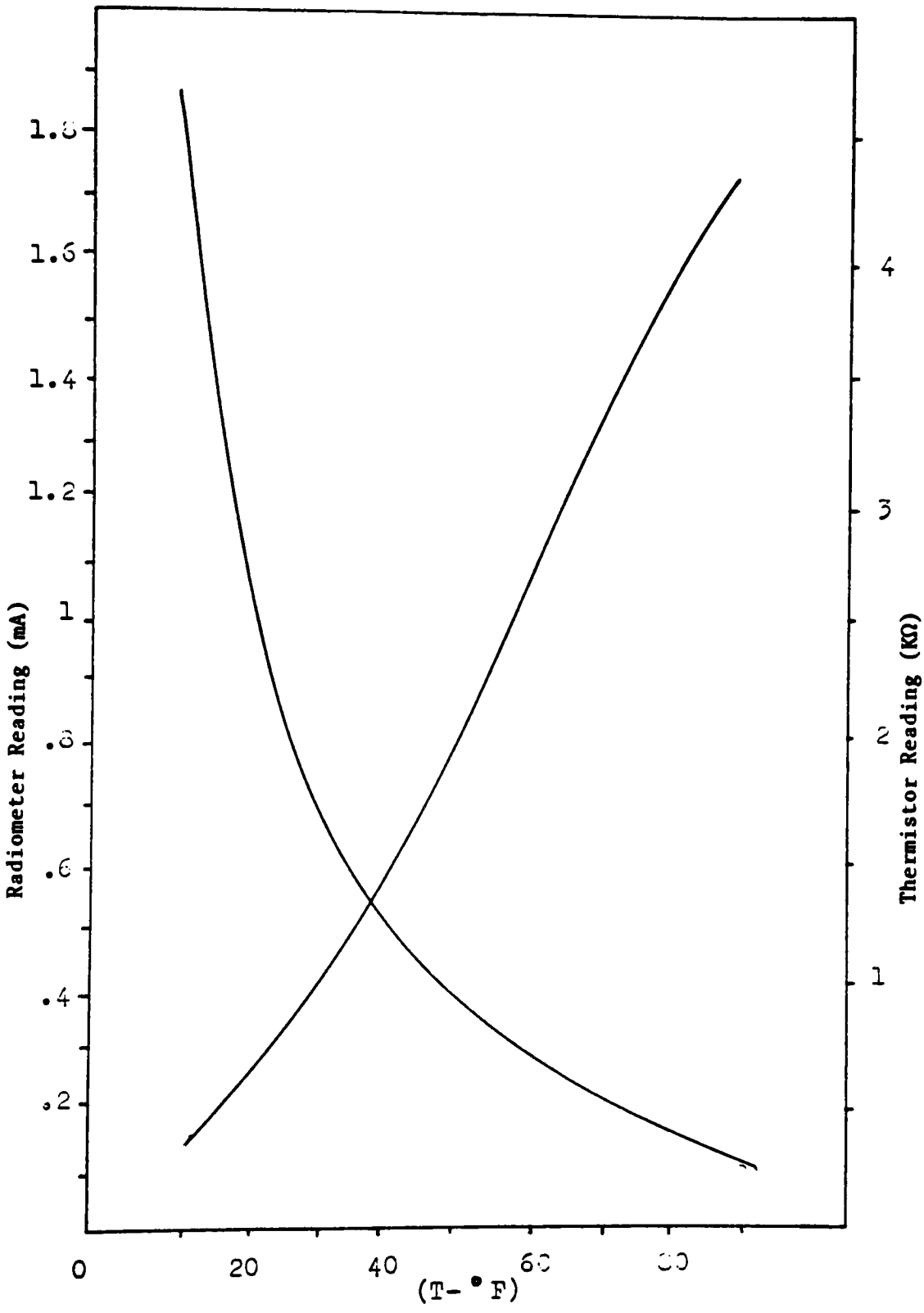

APPENDIX F

Bolometer Calibration Curves

APPENDIX G
Lambertian Assumption Data ($W(0,\phi)$)

	Angle ϕ						
Material	0	10	20	30	40	50	60
Water	0.20	0.14	0.14	0.16	0.20	0.20	0.19
Pavement	0.18	0.18	0.18	0.19	0.19	0.17	0.16
Asphalt	0.18	0.18	0.18	0.18	0.18	0.18	0.20
Concrete	0.18	0.18	0.18	0.18	0.18	0.18	0.19
Grass	0.10	0.14	0.14	0.1	0.12	0.12	0.14
Soil	0.12	0.13	0.12	0.14	0.12	0.15	0.15
Wood	0.16	0.16	0.16	0.16	0.16	0.16	0.16
Brick	0.17	0.17	0.16	0.17	0.17	0.17	0.18

APPENDIX H

Error Analysis

The error analysis was based on methods outlined by Beers and Barford.[3,4] The error accumulates with each variable and the method involves partial derivatives. The method works as follows: Beginning with Equation 17:

$$W_T = \frac{W_0 - RW_S}{\varepsilon} \tag{42}$$

$$S(W_T) = \left[\left(\frac{\partial W_T}{\partial W_0}\right)^2 S(W_0)^2 + \left(\frac{\partial W_T}{\partial R}\right)^2 S(R)^2 + \left(\frac{\partial W}{\partial W_S}\right) S(W_S)^2 + \left(\frac{\partial W_T}{\partial \varepsilon}\right) S(\varepsilon)^2\right]^{\frac{1}{2}} \tag{43}$$

where $S(W_0)$ is the expected error in observed radiance

$S(R)$ is the expected error in surface reflectance

$S(W_S)$ is the expected error in sky radiance

$S(\varepsilon)$ is the expected error in surface emissivity

In Equation 43 partial derivatives are taken with respect to each variable and squared. Then the squared partial derivates are multiplied by the squared error in each variable. The sum of all the squares is taken and the square root of this gives the total error of the variables.

APPENDIX H (continued)

Taking the partial derivatives in Equation 43 gives:

$$S(W_T) = [(\frac{1}{\varepsilon})^2 S(W_0)^2 + (\frac{-W_S}{\varepsilon})^2 S(R)^2 + (\frac{-R}{\varepsilon})^2 S(W_S)^2 + (\frac{W_0 - RW_S}{\varepsilon^2}) S(\varepsilon)^2]^{\frac{1}{2}} \quad (44)$$

Errors on R and ε were taken to be 0.015, and the error on W_S was 5.09×10^{-5}. The error on W_S was based on a 0.2°K temperature error estimate from the specifications on the Barnes PRT 5 radiometer. In equation 42 however, $S(W_0)$ is still unknown. Referring to Equation 16,

$$W_0 = \frac{W(h,0) - W_A}{\tau(h,0)} \quad (45)$$

$$S(W_0) = [(\frac{\partial W_0}{\partial W(h,0)})^2 S[W(h,0)]^2 + (\frac{\partial W_0}{\partial W_A})^2 S(W_A)^2 + (\frac{\partial W_0}{\partial \tau})^2 S(T)^2]^{\frac{1}{2}} \quad (46)$$

$$S(W_0) = [(\frac{1}{\tau})^2 S[W(h,0)]^2 + (-\frac{1}{T})^2 S(W_A)^2 + (\frac{W(h,0)}{\tau^2})^2 S(\tau)^2]^{\frac{1}{2}} \quad (47)$$

The error on W(h,0) falls back on the ability of the detector and this was given as 0.2°K or 1.14×10^{-5} W/cm^2. Errors for both W_A and transmittance had to be calculated. Referring to Equation 28:

$$W_A = \frac{b}{\frac{1}{\cos \phi} - m} \quad (48)$$

APPENDIX H (continued)

$$S(W_A) = [(\frac{\partial W_A}{\partial b})^2 S(b)^2 + (\frac{\partial W_A}{\partial \phi})^2 + (\frac{\partial W_A}{\partial m})^2 S(m)^2]^{\frac{1}{2}} \quad (49)$$

$$= [((\frac{1}{\cos \phi} - m)^{-1})^2 S(b)^2 + (\frac{b (\sin\phi)}{(\frac{1}{\cos \phi} - m)^2 (\cos \phi)^2})^2 S(\phi)^2 \quad (50)$$

$$- (\frac{b(-1)}{(\frac{1}{\cos \phi} - m)^2})^2 S(m)^2]^{\frac{1}{2}}$$

The angle between flight lines was measured with a mask and a ruler accurate to .01". This translates to an error on the angle of .5°. Error on the slope and intercept was calculated during the regression of $W(h,\phi)$ vs. $W(h,0)$ using the following equations:

$$S(m) = \frac{S}{(\Sigma(W(h,0) - \frac{\Sigma W(h,0)}{n}))} \quad (51)$$

$$S(b) = (\frac{\Sigma W(h,0)^2}{n\Sigma(W(h,0) - \frac{\Sigma W(h,0)}{n})^2})^{\frac{1}{2}} S \quad (52)$$

For the error on transmittance, Equation 26 was used where:

APPENDIX H (continued)

$$\tau = \frac{1}{m^{(1/\cos\ \phi)\ -\ 1}} \tag{53}$$

$$S(\tau) = \left[\left(\frac{\partial \tau}{\partial m}\right)^2 S(m)^2 + \left(\frac{\partial M\tau^2}{\partial \phi}\right) S(\phi)^2\right]^{\frac{1}{2}} \tag{54}$$

using the following:

$$\text{let } z = a^y$$

$$\ln z = y \ln a$$

$$dz/z = dy \ln a$$

$$dz = dy\ a^y \ln a$$

and applying Equation 26:

$$m = \tau^{(1/\cos\ \phi)\ -\ 1} \tag{26}$$

$$\ln m = \left(\frac{1}{\cos\ \phi} - 1\right) \ln \tau \tag{55}$$

$$\ln \tau = \left(\frac{1}{\cos\ \phi} - 1\right)^{-1} = \ln m \tag{56}$$

$$-\ln m \left(\frac{1}{\cos\ \phi}\right)^{-2} (\cos\ \phi)^{-2} (\sin\ \phi) = \frac{d\tau}{\tau} \tag{57}$$

APPENDIX H (continued)

$$\frac{d\tau}{d\phi} = -m^{[(1/\cos\theta) - 1]^{-1}} (\ln m) \frac{\sin \phi}{(\cos \phi - \cos^2 \phi)^2} \tag{58}$$

$$\frac{d\tau}{dm} = \frac{1}{\frac{1}{\cos \theta} - 1} \; m^{\frac{\frac{1}{\cos \phi} - 1}{\frac{1}{\cos \phi} - 1}} \tag{59}$$

This results in the following:

$$S(T) = \left[\frac{1}{\frac{1}{\cos \theta} - 1} \; m^{\frac{\frac{1}{\cos \phi} - 1}{\frac{1}{\cos \phi} - 1}} \right]^2 S(m)^2 +$$

$$\left[-m^{[(1/\cos \phi) - 1]^{-1}} (\ln m) \frac{\sin \phi}{(\cos \phi - \cos^2 \phi)^2} \right]^2 S(\phi)^2)^{\frac{1}{2}} \tag{60}$$

Table 3 shows a summary of the error analysis. Points were taken from each set of imagery typical of the upper and lower boundaries of density to represent the full range of measurements of temperature. Once the error in W_T was calculated, a straight linear approximation between radiance and temperature was used around 270°K to convert the error in W_T to error in temperature.

JOHN R. SCHOTT
Calspan Corporation
Buffalo, NY 14225

Temperature Measurement of Cooling Water Discharged from Power Plants

A technique for calibrating a thermal infrared scanner was successfully tested.

INTRODUCTION AND SUMMARY

THE GROWING NUMBER and size of power facilities has stimulated the interest of scientists, legislators, and the public in the effects such stations have on aquatic environments. The impact of thermal discharges on aquatic ecology and the effects on aquatic organisms that are drawn through cooling systems are of particular concern. In order to ensure proper protection and management of the environment as well as continued generation of required power, procedures must be developed to accurately assess environmental effects in a timely and cost-effective manner. In monitoring the cooling water discharged into a water body, the temperature value and spatial extent of the thermal plume are the parameters of interest. These thermal plumes can, in some instances, extend more than a mile from the discharge point and include temperature increases in excess of 15°F.

ABSTRACT: *In an effort to resolve technical, operational, and cost problems associated with the existing approaches for measurement of water surface temperature, a program was initiated to develop and test a wholly airborne calibration of a thermal scanner system as an alternative. This technique involved development of a model relating the signal at the sensor to the surface temperature and the atmospheric effects contributing to the signal at the sensor.*

Procedures were developed for collection and analysis of the thermal imagery such that the terms in this model could be calculated. Once these terms, including atmospheric transmission, sky radiation, and reflectance of the water, have been determined, the water surface temperature can be calculated. In an effort to evaluate this technique, a series of "blindfold" tests were made. In these tests, an airplane flew over a boat located at different positions in the water at different times and on different days. The aircraft values were then compared to the boat values, which had been withheld until the aerial determinations were made. Results of this test indicate that, on the average, the aerial measurements fell within 0.70°F of the boat temperatures (standard deviation ±0.59°F for 63 points). On the basis of these results, this wholly airborne approach, called the "angular calibration technique," is considered operational for airborne measurement of water surface temperatures.

Airborne thermal infrared imaging systems have been used to study some of these problems.[1-3] These systems generate an image (similar to a photograph) of the heat energy radiated by water surfaces. For example, the brighter the water appears on the image, the higher the temperature of the water is. The advantage of this approach is that the thermal scanner can image the entire

PHOTOGRAMMETRIC ENGINEERING AND REMOTE SENSING,
Vol. 45, No. 6, June 1979, pp. 753-761.

APPENDIX I (continued)

surface area of a discharge plume in minutes. In this manner, all the internal detail as well as the shape and spatial extent can be easily determined. The disadvantage of this approach is that a boat is required to provide data needed to convert brightness levels on the image to temperature values.

In an effort to resolve technical, operational, and cost problems associated with the existing approaches, a program was initiated to develop and test wholly airborne calibration of a thermal scanner system so that precise thermal maps could be generated without requiring data from boats. This technique involved development of a model relating the signal at the sensor to the surface temperature and the atmospheric effects contributing to the signal at the sensor.

Procedures were developed for collection and analysis of the thermal imagery such that the terms in this model could be calculated. Data collection procedures included flying the aircraft at different altitudes over the same point in the water and flying parallel flight lines so that data from points in the water could be viewed at different look angles. These procedures add a minimal amount of time to data collection and provide sufficient data so that an analysis of the terms relating water temperature to the signal actually reaching the sensor can be calculated. Once these terms, including atmospheric transmission, sky radiation, and reflectance of the water, have been determined, the water surface temperature can be calculated.

In an effort to evaluate this technique, a series of "blindfold" tests was made.[4] In these tests an airplane flew over a boat located at different positions in the water at different times and on different days. The aircraft values were then compared to the boat values, which had been withheld until the aerial determinations were made.[5] Results of this test indicate that, on the average, the aerial measurements fell within 0.70°F of the boat temperatures (standard deviation ±0.59°F for 63 points). On the basis of these results, this wholly airborne approach, called the "angular calibration technique," is considered operational for airborne measurement of water surface temperatures.

This paper discusses the airborne calibration technique and the experimental test program. For the sake of brevity, the details of the airborne collection system are omitted and the assumption is made that the radiant energy reaching an airborne sensor can be converted to an apparent blackbody temperature equivalent.

Theoretical Approach

Thermal scanners generally detect radiation in the 8-14 μm bandpass. This section will discuss how the radiant energy detected by a sensor at aircraft altitudes (~600 m) is not only a function of temperature but is also functionally dependent on atmospheric and background terms. In addition, the types of measurements required to calculate the values of these additional terms will be defined.

All matter at temperatures above absolute zero radiates electromagnetic energy. The relation between blackbody radiant emittance, W, and temperature, T, in °K is expressed by the Stefan-Boltzmann equation

$$W = \sigma T^4, \tag{1}$$

where σ is the Stefan-Boltzman constant.

The general equation for a blackbody radiator is given by the Planck distribution equation,

$$W_\lambda = 2\pi c^2 h \lambda^{-5} (e^{hc/\lambda kT} - 1)^{-1}, \tag{2}$$

where W_λ is the radiant emittance per unit wavelength interval,

c is the speed of light,
h is Planck's constant,
k is Boltzmann's constant,
T is temperature, and
λ is wavelength.

This equation, derived from quantum physics, is a function of the quantum radiation states within a blackbody cavity.

The Stefan-Boltzmann equation is obtained by integrating the Planck equation over all wavelengths.

The problem in using these equations is finding the dependence of W on temperature over a defined bandpass. The Stefan-Boltzmann equation indicates that radiant emittance integrated over all wavelengths varies as T^4, i.e.,

$$\int_0^\infty W_\lambda \, d\lambda = W = \sigma T^4. \tag{3}$$

To find the functional dependence on temperature in a finite bandpass, it is necessary to use a series expansion solution to the normalized integral of radiant emittance. This yields the fraction of energy less than a given wavelength, D, given by

$$D = \frac{\int_0^\lambda W_\lambda \, d\lambda}{\int_0^\infty W_\lambda \, d\lambda}. \tag{4}$$

APPENDIX I (continued)

These D values are tabulated in standard blackbody tables for ranges of T, λ, or λT combinations.[6] By finding the difference in D for two wavelengths, a relation can be developed between temperature and radiant emittance in a bandpass expressed as a fraction of the total radiant emittance.

If D is the fraction of the total energy emitted by a blackbody between the wavelength 0 and λ, then $D_1 - D_2$ is the fraction of emitted energy between λ_1 and λ_2. Since σT^4 is the total energy for a given temperature, then $W = (D_1 - D_2)\,\sigma T^4$ is the radiant energy emitted for a given bandpass. Values of W and T over the range of interest can be stored in data files on a computer. T can be calculated from the stored W values.

We can therefore express the radiant energy from a blackbody over the 8-14 μm bandpass ($W_{\Delta\lambda}$) as

$$W_{\Delta\lambda} = W_T = \int_{8}^{14} 2\pi c^2 h \lambda^{-5} (e^{hc/\lambda kT} - 1)^{-1}\, d\lambda. \tag{5}$$

This expression, however, is only true for a blackbody. A blackbody is a perfect radiator and absorber; therefore, all the incident energy is absorbed and reradiated. In practice, the bodies we will be concerned with will be gray bodies, which are not perfect absorbers or radiators in the 8-14 μm bandpass and thus have emissivities less than unity.

Emissivity (ϵ) is the ratio of energy radiated from a source to energy radiated from a blackbody at the same temperature. Thus, for a gray body,

$$W = \epsilon\, W_T. \tag{6}$$

In order to interpret the radiant energy reaching a point at any distance from the source, one must consider atmospheric or path effects; of prime concern is atmospheric transmission over the path lengths of interest. The atmospheric transmission window between 8 and 14 μm is the most useful for earth observation work for a number of reasons. It encompasses the radiant energy peak of 9.5 μm for objects near earth ambient temperature of 300°K. The transmission is quite high over the entire window, and the window is spectrally very broad, permitting integration over a sizable fraction of the total energy radiated.

Primary attenuation in the lower atmosphere is due to absorption by H_2O vapor, CO_2, and OH. These molecules absorb the radiation and reradiate it as a function of temperature, thereby introducing two noise terms into the system.

These terms can be included in the expression we have defined as follows:

$$W = \tau\epsilon W_T + W_A \tag{7}$$

where τ is the atmospheric transmission and W_A is the apparent radiant emittance from the air column between the source and sensor, as well as energy scattered into the sensor. It is important to keep in mind that W_A and τ vary as a function of atmospheric conditions on a given day and also within the air column because of layering effects in the atmosphere.

In addition to the radiant energy from the source itself, a certain amount of energy will be reflected from the ground. This energy comes from both the sun and the sky. Solar reflection effects can be avoided by proper orientation of flight lines. Skylight reflection effects can be expressed as $W_s\,\tau R$ and included in Equation 7, yielding

$$W = \tau\epsilon W_T + W_A + W_s\,\tau R \tag{8}$$

where W_s is the radiant energy from the sky incident on the surface observed, and can be associated with an equivalent sky temperature, T_s. R is the surface reflectance of the water.

Skylight irradiance comes from scattered solar radiation, radiation emitted from components of the atmosphere (especially the ozone layer and H_2O vapor), and energy from the Earth reflected by the atmosphere. All these effects combine to give the sky an apparent radiometric temperature as viewed from the ground. For our purposes, this is the blackbody temperature equivalent, T_s, associated with the amount of energy incident on the source over the bandpass of interest. T_s can vary considerably with sky conditions from about 300°K for heavy overcast to well below 250°K for clear sky conditions.

In evaluating the range of values for the reflectance terms, we recognize that reflection is dependent on look angle. In addition, we have mentioned that W_A and τ are dependent on the length and composition of the atmospheric path between the source and observation point. To recognize this dependence in Equation 8, the functional dependence on θ and h will be added to designate angular and height dependence, respectively,

where h is the height of sensor above terrain,
θ is look angle measured from the vertical, and

APPENDIX I (continued)

$$W(h,\theta) = \tau(h,\theta)\,\epsilon(\theta)\,W_T + W_A(h,\theta) + \tau(h,\theta)\,W_s\,R(\theta). \quad (9)$$

Limiting our discussion for the moment to vertical viewing, ($\theta = 0$), results in

$$W(h) = \tau(h)\epsilon\,W_T + \tau(h)\,W_s\,R + W_A(h). \quad (10)$$

Letting $W(0)$ be the energy from the ground as it would be measured vertically at zero altitude, Equation 10 reduces to

$$W(h) = \tau(h)\,W(0) + W_A(h) \quad (11)$$

where $$W(0) = \epsilon W_T + W_s R. \quad (12)$$

If $W(h)$ and $W(0)$ are known for a set of observed values, then, by least-squares analysis of Equation 11, $\tau(h)$ and $W_A(h)$ can be calculated. $W(h)$ and $W(0)$ represent the radiant energy observed by the sensor at flight altitude and ground level, respectively. In practice, the ground level measure is obtained by extrapolating a plot of altitude-versus-temperature to zero altitude using data collected over the same point at a series of altitudes, where radiant energy is converted to apparent blackbody temperature.

If we once again consider the angular viewing effects, Equation 11 becomes

$$W(h,\theta) = \tau(h,\theta)\,W(0,\theta) + W_A(h,\theta) \quad (13)$$

where

$$W(0,\theta) = \epsilon(\theta)\,W_T + W_s\,R(\theta), \quad (14)$$

$$\tau(h,\theta) = \tau(h,0)\ \exp\,(1/\cos\,\theta), \text{ and} \quad (15)$$

$$W_A\,(h,\theta) = W_A(h,\,0)/\cos\,\theta. \quad (16)$$

These equations result from the increase in absorption with path length (Equation 15) and the increase in atmospheric radiation with path length (Equation 16). Since the path length increases as $1/\cos\,\theta$ for slant viewing and the effects on atmospheric emissions should be very nearly linear for small increases in path length through a given medium, Equation 16 is derived. Note that this assumption of linearity is only valid for increase due to slant viewing through a known atmosphere and is not necessarily valid for an overall increase in path length.

If observations were made at the same altitude of a given point through two different look angles, one of which may be taken as vertical for convenience, then Equations 10, 13, and 14 may be combined to yield

$$W(h,\,0) = m\,W(h,\,\theta) - m\tau(h,\,\theta)\,W_s\,R(\theta) - m\,W_A(h,\theta) + \tau(h,\,0)\,W_s R(0) + W_A(h,\,0) \quad (17)$$

where $$m = \frac{\epsilon(0)\,\tau(h,\,0)}{\epsilon(\theta)\tau(h,\theta)}. \quad (18)$$

Recognizing this as a straight line in the form,

$$W(h,\,0) = mW(h,\,\theta) + I \quad (19)$$

and solving for W_s in terms of m and I yields

$$W_s = \frac{I + mW_A(h,\theta) - W_A(h,\,0)}{\tau(h,\,0)\,R(0) - m\tau(h,\theta)\,R(\theta)}. \quad (20)$$

Least-squares analysis of Equation 19, with input data consisting of apparent temperatures (converted to radiant energy) measured along a line viewed vertically and then at a slant angle, will yield from Equation 20 a measure of apparent sky temperature as viewed from the ground.

We have assumed that the apparent temperature of the sky is a constant with respect to angle of observation. In general, this is not the case; rather, the zenith sky appears colder than the sky near the horizon because the atmosphere viewed vertically has fewer radiators. Because of the variability of sky conditions, a functional relationship between sky temperature and view angle is not readily defined nor are the errors introduced by the assumption of a constant sky easily evaluated. In order to minimize potential errors in measured sky temperature, the analysis discussed above can be conducted for a number of look angle combinations, and a simple relationship between T_s and θ can be developed.

Another solution would involve use of a vertical-viewing, upward-looking radiometer on board the aircraft. Measurement of vertical sky temperature at a number of altitudes and extrapolation to the apparent temperature of the nadir sky as viewed from the ground would eliminate one unknown in Equation 17. The equation could then be solved for the sky temperature at look angle θ (i.e., T_s associated with $R(0)$ would be known and T_s associated with $R(\theta)$ would be unknown).

Rewriting Equation 9 as

$$W_T = [W(h,\theta) - \tau(h,\theta)\,W_s\,R(\theta) - W_A\,(h,\theta)]/\epsilon(\theta)\,\tau(h,\theta), \quad (21)$$

we find

$W(h,\theta)$	is a measured value;
$W_A(h,\theta)$	is obtained from Equation 16 and least-squares analysis of Equation 11;
$\tau(h,\theta)$	is obtained from Equation 15 and least-squares analysis of Equation 11;

W_s is obtained from Equation 20; and

$R(\theta)$ and $\epsilon(\theta)$ are tabulated values for water.

It should therefore be possible to measure the absolute value of surface waters based on the theories developed thus far. The next section contains procedural approaches for collection of necessary input data to solve for the values in Equation 21.

Experimental Design

Our concern at this point is in defining procedures for collecting sufficient input data to permit the use of the theoretical procedures under discussion. Again, we will neglect, for simplicity, signal processing through the sensor and assume that apparent blackbody radiometric temperature can be measured at the sensor location by converting radiant energy to equivalent blackbody temperature.

As shown in Equation 11, the input data necessary to calculate the transmission term $\tau(h)$ and the additive target-independent energy from the atmosphere $W_A(h)$ consist of $T_B(h)$ and $T_B(0)$ corresponding to $W(h)$ and $W(0)$. $T_B(h)$ is simply the apparent blackbody temperature measured at altitude h with look angle $\theta = 0$. $T_B(0)$ is the apparent temperature measured at the surface of the water. This value cannot be measured directly but is obtained by a profile technique which involves a simple extrapolation process for data collected at a series of altitudes to a zero altitude case obtained by consecutive flights over the same target.[7] A target consists of an area of uniform temperature either large enough to be directly below the aircraft during the profile or within about 10° from the nadir and distinct enough to be identifiable on the profile images. At angles much larger than 10° the assumption of vertical viewing during the profile no longer holds.

The minimum data input required for Equation 11 is $T_B(h)$ and a corresponding $T_B(0)$ for at least two points at differing temperature. Ideally, these data consist of a set of approximately five data points covering as wide a temperature range as possible. Figure 1 indicates how $T_B(h)$ and $T_B(0)$ could be obtained for a number of different temperatures.

The input data necessary to calculate W_s, the sky radiance term, comes from the solution of Equation 19, requiring $T_B(h, 0)$ and $T_B(h,\theta)$ as inputs. These values are the apparent temperature observed at the same point through two look angles where one look angle is chosen as zero degrees for convenience. (Note also that Equation 11 can be solved directly for W_s, i.e., a one point solution is available). The minimum data required to solve Equation 19 consist of two data sets composed of $T_B(h,0)$ and $T_B(h,\theta)$ for two distinct points. In general, a number of points with a large range in temperature should be used to solve for m and I in Equation 19. This data set can be collected by flying two parallel flight lines and allowing for some sidelap. This procedure is often used to obtain complete target coverage and would add little or no time to most collection efforts. Figure 2 illustrates how these data could be obtained.

A ground-truth program was used to evaluate these radiometric calibration techniques. This effort involved aerial overflights of a boat anchored at a series of positions in the Hudson River, both within and beyond the thermal plumes of various power plants.

With the boat anchored at a given position, readings were made on the upstream (downstream if flow was upstream in the estuary) side of the boat. Measurements consisted of temperatures recorded from a submerged thermistor (nominally at a depth of 6 in.) and from a Barnes PRT-5 radiometer. During each fly-over, approximately ten readings were recorded and averaged to predict the temperature at a point. To insure unbiased data, all surface measurements were made by independent consultants and surface data were withheld until aerial results had been delivered to the New York State Energy Research and Development Authority (NYSERDA). The surface radiometer was calibrated in the field under prevailing atmospheric conditions to ensure that all measurements were absolute surface temperature measurements.

The main survey took place on September 24, 1976 with the boat anchoring at eight positions throughout the day. The aircraft flew over each position four times, permitting 32 data-comparison points for the total survey. Because the boat was covered with aluminum foil, it had a low emissivity and could be located as a "cold" spot on the image. Surface temperatures were predicted using the calibration technique discussed above. Data were also collected at eight positions for five overflights on both July 8 and 9, 1976. However, the July 8 data could not be used because of calibration problems with the surface instrument.

APPENDIX I (continued)

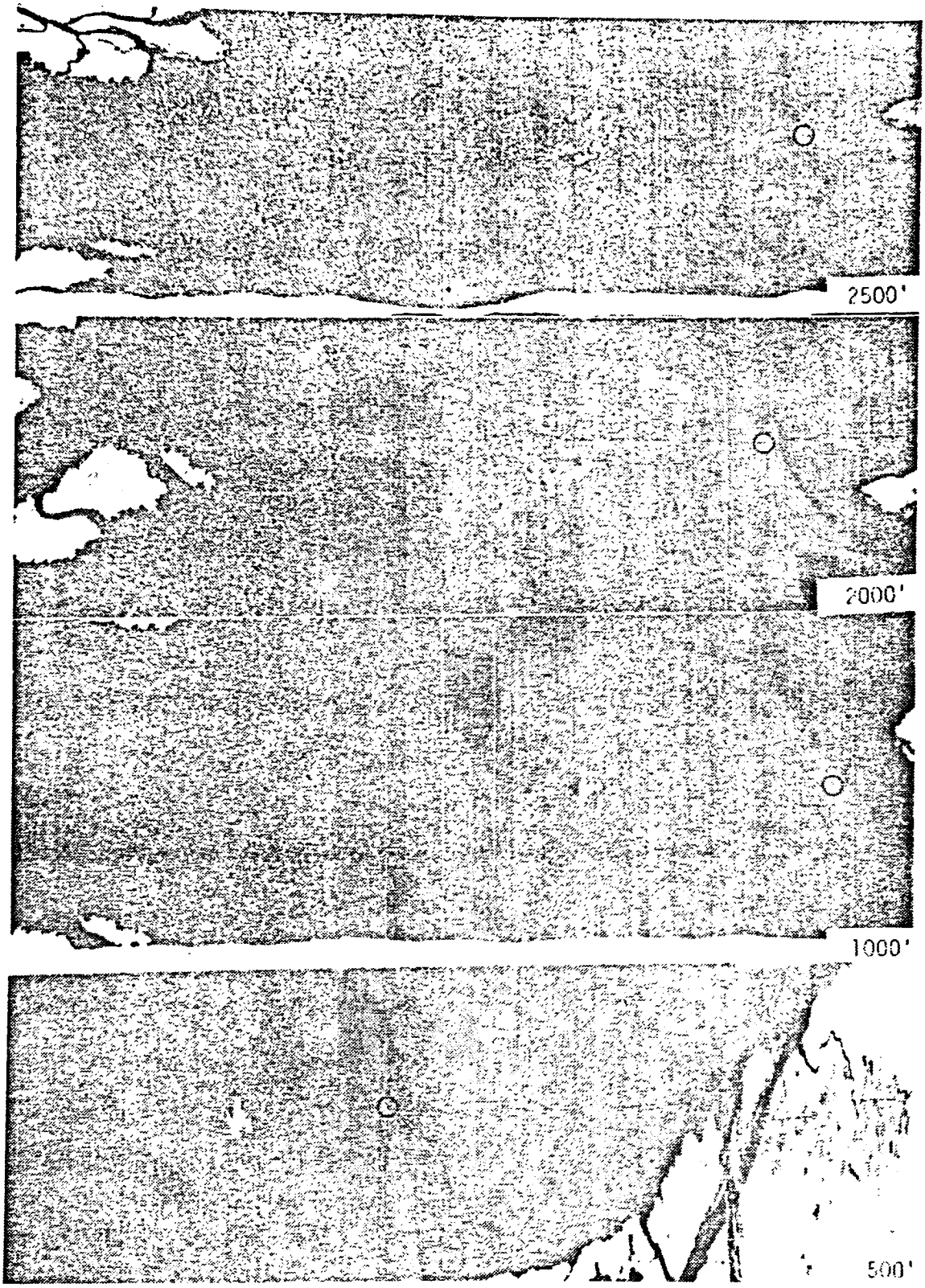

FIG. 1. Thermal images obtained during a profile. Areas of equal temperature where apparent temperature readings could be made are indicated.

APPENDIX I (continued)

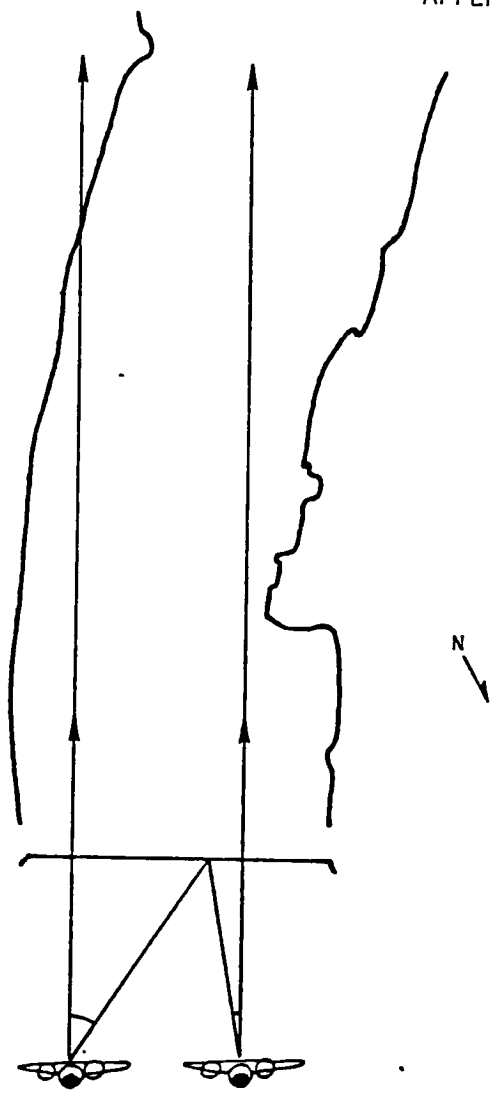

FIG. 2. Example of parallel flight lines over a power station showing the change in look angle for a given ground point.

RESULTS

Table 1 presents the results of the data correlation for September 24. The mean and standard deviations of the absolute value of the difference between the aerial and surface data are presented. Radiometric surface data were used because they are a more accurate measure of the actual surface temperatures than is the submerged thermistor. Comparison of submerged (6 in.) thermistor data and aerial data showed a mean difference of 0.51°F with a standard deviation of ±0.46°F. Also included is a correlation of radiometric temperatures, to which no atmospheric correlations have been applied, with the surface data. Table 2 contains the results of the July 9 survey.

When the July and September data are combined, a mean error of 0.70°F is obtained with a standard deviation of ±0.59°F (Angular Technique). This compares with a mean error of 3.23°F with a standard deviation of ±1.25°F if only internal system calibration is used. Figure 3 illustrates the precision of the calibration technique and the limitations of using only internal scanner calibration. The figure shows the surface radiometer data plotted against the calibrated (*) and uncalibrated (□) scanner data. The data, which have been corrected for atmospheric and background effects, show a very close fit within the 1°F error bars. The data using only the internal scanner calibration show sizable errors and are generally less than the actual temperature. Note that this is generally the case but that a temperature higher than the true surface temperature can be detected by airborne systems under certain atmospheric and background conditions.

One shortcoming to the angular technique is a requirement for extra data to permit calibration and some additional data processing. Neither the time nor the cost is appreciable; however, the data must be properly collected. Some improvements in accuracy could be expected if data collection were modified to facilitate analysis using the angular technique. Major improvements cannot be expected because temperatures predicted from the air approach the accuracies obtainable by surface measurements.

CONCLUSIONS AND RECOMMENDATIONS

The data correlation results presented in the previous section indicate that a major advance in airborne radiometric measurement of water surface temperatures has been achieved.[8] Measurement accuracies essen-

TABLE 1. COMPARISON OF SURFACE AND AERIAL DATA FOR 24 SEPTEMBER 1976 (°F)

	Surface Radiometer and Uncorrected Airborne Scanner	Surface Radiometer and Angular Technique
Mean of the absolute value of the temperature difference between boat and aircraft.	4.19	0.55
Standard deviation of ΔT	±1.22	±0.57

APPENDIX I (continued)

TABLE 2. COMPARISON OF SURFACE AND AERIAL DATA FOR JULY 9, 1976 (°F)

	Surface Radiometer and Uncorrected Airborne Scanner	Surface Radiometer and Angular Technique
Mean of the absolute value of the temperature difference between boat and aircraft	2.66	0.80
Standard deviation of ΔT	±1.27	±0.57

tially as good as surface measurements are demonstrated.

The data collection procedures involve only minor variations in standard collection practices requiring approximately 15 additional minutes of flight time. All data processing can be done on a desk-top computer.

The net result of these conclusions is that a fully airborne approach to measure water surface temperatures, with accuracies comparable to those obtained from surface measurements, is an operational possibility. In addition, these results were obtained through use of an outside consultant for acquisition of ground-truth data, thus precluding any bias.

We recommend that future efforts in this area be directed at techniques to generate thermal maps with appropriate corrections at angles away from vertical. The corrections developed using the angular calibration techniques are quite accurate and should be applied in map generation. Current mapping techniques do not apply a correction for variations in apparent temperature at non-vertical look angles; development of these corrective procedures in the map-generation process would allow the full accuracies developed in the angular calibration technique to be carried through to a final map product. In addition, data collected specifically for analysis using this technique should eliminate the need for iterative solutions and should further improve calibration accuracies. While major improvements in water temperature measurements could not be expected because the current results already so closely approach surface measurements, improvements applicable to such problems as a quantitative measurement of heat loss from buildings could be expected. In fact, a major advantage of this technique is that it includes consideration of sufficient variables

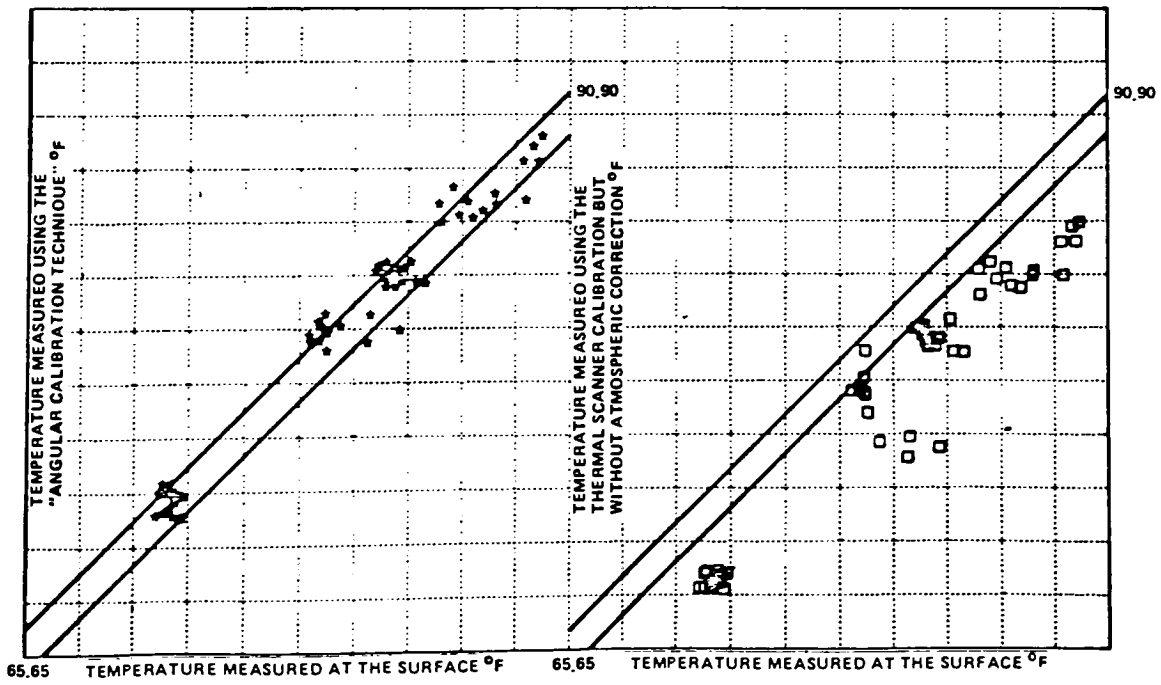

FIG. 3. Comparison of surface and aerial temperature measurements (the lines represent a 1°F error envelope).

to allow surface temperature measurement of any uniform flat surface whose emissitivity is known.

ACKNOWLEDGMENT

The work reported was sponsored by the New York State Energy Research and Development Authority (NYSERDA) under an agreement dated August 23, 1976 with Calspan Corporation.

REFERENCES

1. Bartolucci-Castedo, L. A., *et al.*, *Computer Aided Processing of Remotely Sensed Data for Temperature Mapping of Surface Water from Aircraft Altitudes*, LARS Publication, Purdue University, Indiana, 1973.
2. Haynes, R. B., and J. Whipple, *Problems in Applying Infrared Reconnaissance Technology to Water Temperature Surveillance*, Technical Memorandum No. RADC/IR/TM-71-2, 1971.
3. Scapace, F. L., R. P. Madding, and T. Green III, *Scanning Thermal Plumes*, Ninth International Symposium on Remote Sensing of Environment, April 1974.
4. Schott, J. R., *Thermal Remote Sensing Calibration Techniques*, Calspan Report NA-6019-M-1, NTIS #TB-269-471, 1977.
5. *Report of Infrared Water Temperature Measurements Made September 24, 1976 of the Hudson River*, Wormser Scientific Co. Report, Stamford, Connecticut.
6. Pivovonsky, M., and M. R. Nagel, *Tables of Black Body Radiation Functions*, The MacMillan Company, New York 1961.
7. Schott, J. R., and R. H. Tourin, "A Completely Airborne Calibration of Aerial Infrared Water Temperature Measurements," Proceedings *ERIM Tenth International Symposium on Remote Sensing of Environment.*
8. Schott, J. R., and T. W. Gallagher, "Profile Technique For Calibration of Infrared Thermal Imaging Systems" U.S. Patent 3,970,848 July 20, 1976.

(Received January 4, 1978; revised and accepted February 28, 1979.)

VITA

The author of this paper is presently a member of the Canadian Armed Forces (CAF), currently the rank of Captain. His specific area of employment is in the Aerospace Engineering classification with specialities in armament and photography.

Capt. Macleod was born in Peterborough Ontario. Immediately following completion of high school, he joined the CAF and went to Royal Military College (RMC) for training during the next four years. In 1977, he graduated from RMC with a BEng in Mechanical Engineering.

From 1977 to 1981 Capt. Macleod was employed at Canadian Force Base Cold Lake as a maintenance manager for aircraft systems and personnel in support of photographic, armament and aircraft servicing operations. In 1980 Capt. Macleod obtained, through examination, Professional Engineers status with the Association of Professional Engineers, Ontario, Canada (APEO). In 1981 he applied for and was accepted for advanced training at Rochester Institute of Technology. Academic studies were completed and this study was undertaken as required for a master's degree in Photographic Science and Instrumentation.

In December, 1982 Capt. Macleod was transferred to National Defense Headquarters, Ottawa, Ontario, where he is responsible for current photographic systems in the CAF.